Characterization and Design of a Fibrotic Tissue Surrogate

Emma C. Bédard

Department of Chemical Engineering McGill University

SoundBite Medical

Montréal, Québec, Canada

April 2018

A thesis submitted to McGill University in partial fulfillment of the requirements of the degree of Master of Engineering

Abstract

Chronic total occlusions (CTO) are complete blockages of arteries characterized by a high risk for heart attacks, stroke and limb loss. The occlusion is composed of collagen-rich extracellular matrix, intra and extracellular lipids, smooth muscle cells and mixed components, including cholesterol, dense collagen and calcium deposits. As a result, these lesions are extremely heterogeneous and cannot be easily reproduced ex-vivo for the purposes of medical device testing. Current pre-clinical testing and new device validation is performed using cadavers or amputated limbs which can be difficult to obtain in substantial quantities. Animal models, where occlusions are difficult to create and where time and costs become a serious constraint.

In the interest of accelerating the development of the SoundBite Medical Active Wire^{TM} crossing technology, the primary goal of this thesis was to study and characterize the mechanical properties of fibrotic-tissue-rich plaques retrieved from cadaveric femoral arteries to propose a surrogate, or a class of surrogates, that can mimic the response and behavior of these complex fibrotic plaques when subjected to percutaneous intervention with a guide wire. It was found that artificial or synthetic surrogates are not suitable for reproducing the behavior of this complex tissue. Biological surrogates, such as bovine pericardium and chicken skin provide adequate resemblance to fibrotic tissue found in plaques and could, with some modifications, provide a viable medium to test and optimize a percutaneous intervention device.

Abrégé

Les occlusions totales chroniques (CTO) sont des bloquages complètes d'artères caractérisés par un risque élevé d'infarctus et d'accidents vasculaires cérébraux (AVC). Les CTO peuvent être composées d'une matrice extracellulaire riche en collagène, lipides extracellulaires et cellules musculaires lisses ainsi que d'autres composantes telles que le cholestérol et tissus fibrosés à densités variées ou à divers degrés d'organisation et de dépôts de calcium. Par conséquent, les CTO sont des structures grandement hétérogènes qui ne peuvent pas être reproduites ex vivo en laboratoire. Pour valider de nouvelles technologies médicales, les tests préliminaires sont donc réalisés à l'aide de dépouilles humaines ou de membres amputés qui ne sont pas toujours disponibles en grand nombre et ne garantissent pas des tissus frais, ni totalement représentatifs mécaniquement. Il est possible d'utiliser des tissus provenant des sources animales pour pallier à la rareté et aux lacunes des dépouilles humaines, mais la culture d'analogues biologiques souhaités requiert souvent des semaines de préparation et entrâine des coûts exorbitants.

Le but principal de la présente thèse est de définir et caractériser les propriétés méchaniques du tissu fibreux dans les CTO d'artères fémorales cadavériques afin de proposer un ou des analogues ayant un comportement mécaniquement semblable sous la force compressive d'un fil guide et détenant des propriétés matérielles comparables, ceci dans le but d'accélérer le développement de la technologie Active Wire^{TM} de SoundBite Medical. Il a été constaté que les analogues artificiels ou synthétiques ne sont pas des modèles adéquats du tissu fibrosé. Tandis que les analogues biologiques, tels que le péricarde bovin et la peau de poulet, offrent une vraisemblance méchanique avec le tissu fibrotique dans les occlusions chroniques et peuvent, avec des modifications, constituer un médium viable afin tester et d'optimiser une nouvelle technologies en intervention percutanée.

ACKNOWLEDGEMENTS

"Two roads diverged in a yellow wood,

And sorry I could not travel both

And be one traveler, long I stood

And looked down one as far as I could

To where it bent in the undergrowth;

I shall be telling this with a sigh

Somewhere ages and ages hence:

Two roads diverged in a wood, and I—

I took the one less traveled by,

And that has made all the difference."

-Robert Frost

It's funny how a single conversation with a stranger at an Easter lunch can turn into a complete career change and into this thesis. Professor Leask, you are no longer a stranger and I still am in awe at how you so easily convinced me to pursue a Masters degree in a field I never thought I'd pursue. I can't thank you enough for giving me a spot in your group, exposing me to the fascinating world of cardiovascular mechanics and living through the tumultuous roller coaster of being the first grad student to (hopefully) obtain the Surgical Innovation Certificate!

Un TRÈS GROS remerciement à Louis-Philippe Riel, Martin Brouillette, Steve Arless et toute la gang chez SoundBite Medical. Merci de vouloir m'accommoder durant le stage l'été dernier comme étudiante de McGill (et non Sherbrooke...) ainsi d'être patient avec toutes mes compétitions de vélo et d'aviron, mes blessures et de vouloir prolonger le stage en ce qui est devenu quasiment un an de travail à titre de stagière! Ce fût une opportunité phénoménale et j'ai beaucoup de respect pour votre équipe, votre technologie et ce que vous êtes en train de bâtir.

A big shout out to Jonathan Unno for being the whiz he is at nanoindenting, for being so patient and available during the indenting blitz! I'd also like to thank Lisa Danielczak for helping me around the lab and teaching me the secret to making agar. To Roya Jamarani, thanks for being an amazing friend, keeping me sane and reassuring me that I wouldn't fail out and become a vagabond. To Keith Wakeham, thanks for the MatLab code debuggery and the motivational chirping from the Italian north. À Claire, je te remercie pour les bons conseils de français et les corrections de l'abrégé. And last but not least (because even oscar winners thank their parents) a huge thanks to mom and dad for the unconditional love and encouragement but mostly for giving me a place to live, do laundry and a pantry of food during this McGill adventure. With a degree in hand though, it might be time to move out!

Contents

List of Abbreviations and Symbols

CTO	Chronic total occlusion
PCI	Percutaneous coronary intervention
PPI	Percutaneous peripheral intervention
CABG	Coronary arterial bypass graft
PVD	Peripheral vascular disease
L-PLA	L-polylactic acid
SMC	Smooth muscle cell
TCFA	Thin-capped fibrous atheroma
ECM	Extracellular matrix
Micro-CT	Micro computed tomography
SSI	Supersonic Shear Imaging
μ	Shear modulus
c_s	Shear wave speed
ρ	Tissue density
E	Elasticity (Young's Modulus)
UTN	United Tissue Network
CRCHUM	Centre de Recherche du Centre Hospitalier de l'Université de Montréal
OCT	Optimum Cutting Temperature
IRIC	Institut de Recherche en Immunologie et Cancerologie
ROI	Region of interest
HU	Houndsfield unit
SD	Standard deviation
STP	Standard temperature and pressure
HPS	Hematoxylin Phloxine Saffron

MT	Masson's Trichrome
GAG	Glucosaminoglycans
R	Radius of the indenter tip
h_c	Contact depth
h_{max}	Maximum indent depth
r	Radius of the projected contact area of the tip with substrate
E_r	Reduced modulus
H	Hardness
S	Unloading stiffness
P	Force
A_p	Contact area
υ_i	Poisson's ratio of the indenter
υ_s	Poisson's ratio of the substrate

1 Motivation and Background

1.1 Introduction

Until recently, to revascularize a region with a chronic total occlusion (CTO) bypass was needed to "plumb" around the blockage. However, technologies in endovascular treatment (percutaneous coronary intervention (PCI) and peripheral interventions (PPI)) provide the ability to minimally-invasively address more complicated lesions and an expanding number of more acute situations [1]. However, the treatment of CTOs still remains hotly debated between surgery or percutaneous intervention due to a considerable variety of unsettled issues in field of CTOs as a target for revascularization procedures; CTOs still remain the lesion subtype in which PCI and PPI are most likely to fail. Despite these obstacles, several studies have documented that successful PCI of CTOs leads to an improvement in anginal status, normalization of functional tests, improvement of left ventricular function and avoidance of cornoary bypass surgery (CABG) [2, 3]. In the case of peripheral vascular disease (PVD), successful PPI of CTOs maintains all options for extremity revascularization, allows for preservation of the saphenous veins for future use (extremity or CABG), requires no general anesthesia, improves limb functionality and has a lower rate of morbidity [4]. However, improvements are still needed in percutaneous interventional crossing technologies and techniques to increase the success rates.

To address this need, new crossing technologies are emerging and are driving the necessity to develop accurate CTO models whether as in vivo animal models or as benchtop surrogates. Sim et al. [5] managed to create porcine coronary CTOs using implanted wire stents and bioabsorbable L-polylactic acid polymer (L-PLA), however 13 out of 20 pigs in their study died prematurely of stent thombosis and the fully developped model took 4-5 weeks post-implantation for it to be a viable testing medium. This is a costly and risky option for early device testing. In another attempt to create an animal CTO model, Frie et al. [6] designed an

interventional method of placing a bone marrow plug with a patent lumen in pigs, either in the coronary or peripheral arteries. Again, this model is limited by requiring post-implantation time of up to 3 weeks and only simulating the properties of a calcific chronic partial occlusion, which doesn't fully mimic the representative mechanical behaviors of chronic total occlusions. Other research groups used surrogates such as layers of various concentrations of agar or gelatine [7], however this also fails to represent a softer CTO as the gels are simply too homogenous. An effective in vitro testing model is needed.

1.2 Chronic Total Occlusions

The pathophysiological mechanism of an occlusion begins with the process of atherosclerosis, as demonstrated in figure 1. Described as a low-grade inflammatory state of the inner lining of arteries, atherosclerosis occurs over time and is accelerated by risk factors such as diabetes, high blood pressure, smoking, high cholesterol levels and genetics [8]. An atherosclerotic plaque is composed of inflammatory cells, cellular debris, smooth muscle cells (SMCs), and varied amounts of cholesterol and cholesterol ester, some of which is in the form of cholesterol crystals. This lipid core forms in some plaques under a fibrous cap composed primarily of collagen. The cap is covered on its luminal side by a single layer of endothelial cells as is the inner layer of all arteries within the body. An abundance of inflammatory cells derived foam cells originating from circulating monocytes migrate into the arterial wall and may weaken and thin out the fibrous cap. These plaques are termed thin-capped fibroatheromas (or TCFAs). These processes can ultimately result in a tear in the cap, exposing the thrombogenic lipid core under the cap to the flowing blood, leading to the formation of an intraluminal thrombus. Depending on several factors, including the plaque composition, plaque volume and the degree of luminal narrowing, size of the cap tear, and the thrombotic milieu, the thrombus that forms may either lyse spontaneously, remain, and sub-

sequently be incorporated into the wall of the artery (further narrowing the lumen) or grow and progress to total or near coronary occlusion and a symptomatic acute coronary event [8].

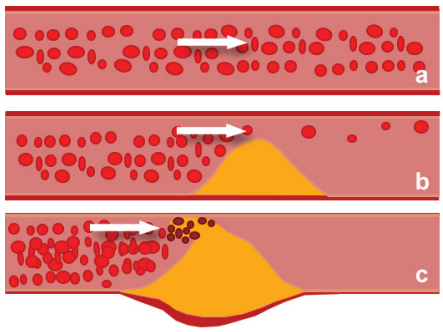

Figure 1: Progression from (a) healthy artery to (b) an atherosclerotic artery to (c) an occluded artery

CTOs are complete blockages (hence known as occlusions) of arteries characterized by a high risk for heart attacks and stoke, with no antegrade flow beyond the point of occlusion [9]. The core composition correlates with the age of the CTO. Older occlusions have higher concentration of fibrocalcific material (defined as "hard plaques"), while CTOs aged less than one year have more cholesterol clefts and foam cells among other less-fibrous materials. Typically, CTOs may be classified as soft, hard or a mixture of both. CTOs are a common find; typically detected in 18-52% in diagnostic coronary angiograms [2]. With time, collagen replaces thrombus and lipids, especially at proximal/distal ends or caps. Increasingly dense fibrous collagen and calcification occurs.

1.3 CTO Crossing & New Device Testing

SoundBite Medical Solutions (Montreal, QC) is developing a proprietary CTO crossing system, a unique wire-based technology that may potentially allow the

treatment of CTOs in a simpler and clinically efficient way. Specificially, their device delivers targeted shockwaves, enabling the crossing of challenging and highly calcified CTOs while leaving healthy elastic tissue unharmed. Cadaveric samples, animal models and ex-vivo samples are currently used for pre-clinical testing and new device validation. Since these biological tissues are difficult to obtain in significant quantity and are inherently variable, it is one of SoundBite's desires to find a representative ex vivo CTO surrogate to allow repeatable testing models that cost-effectively accelerate research and development activities.

Most of the current work in the scientific and engineering community testing crossing devices has been to evaluate the vulnerability or stability of an atherosclerotic plaque (and CTOs) [10, 11, 12, 13]. However, as Riel et al. [14] point out in their study, none of these studies recommend an experimental artificial analogue to validate theoretical results. Data on the material properties of CTOs is sparse. Riel et al. were able to demonstrate and characterize some mechanical properties of medial calcification from older and hardened CTO plaques however this is still insufficient characterization work to fully understand the mechanochemical and biological properties of a whole plaque. For example, it is as important to understand the properties of an occlusion that is deemed "soft"; as in a total occlusion that is in the process of maturing. Such a process is analogous to the process of wound healing on the surface of the epidermis, which is characterized by the replacement of an initially proteoglycan-rich extra-cellular matrix (ECM) into a collagen-rich scar as well as the neovascularization process that is characteristic to occluded veins and arteries [15]. This presents itself as a difficult yet highly relevant challenge of analyzing these soft plaques and their mechanical properties to be able to create a surrogate, fully-encompassing experimental model that is useable and reproducible for testing CTO crossing devices and equipment for these plaques that are softer and not as calcium-dense as older lesions.

1.4 Imaging and Characterization Techniques

To evaluate the material properties of CTOs, a variety of images and ex vivo techniques can be used. Imaging techniques of interest include various types of microscopy: scanning electron microscopy, in situ fluorescent microscopy, colormetric assays, as well as 2nd-harmonic generation imaging, magnetic resonance imaging, micro-computed tomography and elastography in addition to histology. Mechanical characterization of biological materials can be achieved through various techniques such as atomic force microscopy, rheometry, bi-axial tensile testing, nanoindentation, among others. However, due to budgetary, time and availability constraints in conjuction with a strict corporate-mandated collaboration, the background provided is limted to only the techniques utilized within this research. These techniques were selected to provide adequate introductory characterization and clinically-relevant material behavior. The following is a brief introduction to the techniques chosen to fulfill the research objectives.

Micro-Computed Tomography (Micro-CT)

Micro-CT is an advanced imaging modality that enables viewing a specimen in three dimensions on a small scale with very high resolution. It does not require any sample preparation nor any histological slicing. Using a micro-CT scanner, the internal structure of a tissue can be visualized without destroying the sample tissue. This technology is useful for nondestructively visualizing and analyzing the internal structure of materials such as soft tissues, dense tissues, bones or calcified zones in arteries. Micro-CT is an x-ray transmission image technique, where x-rays are emitted from a generator, travel through the sample and are recorded by a detector on the other side. The sample is then rotated by a fraction of degree and another projection image is taken at the new positions [16]. The procedure is repeated until the sample has rotated either 180° or 360° producing a series of slice-by-slice images.

Elastography

Supersonic Shear Imaging (SSI), a dynamic elastography method, is an ultrasound system that gives a real-time and quantitative two-dimensional map of tissue stiffness. Image processing in SSI consists of applying the cross-correlation algorithm to all the images acquired after pushing and to the reference image. This process is used to determine the degree of medium displacement due to propagation of the shear wave. It is possible to obtain the shear modulus (µ) of the medium from the images of the wave displacement over time [17, 18]. In tissues, a shear wave induces particle movement perpendicularly to the direction of wave propagation with a speed of approximately a few meters per second (less than 30 m/sec) [19]. The shear wave speed (c_s) is directly related to the shear modulus: $\mu = \rho * c_s^2$ [19], where ρ is the biological tissue density (1,000 kg/m^3) under the assumptions of a pure elastic and isotropic medium. However, for incompressible media (which includes most biological tissues) µ is approximately one-third of the Young's modulus (E). Therefore, by assuming a purely elastic medium and a standard density of 1,000 kg/m^3, the shear wave speed can be used to obtain the E according to $E = 3\rho^* {c_s}^2$[20], which means the values of the Young's modulus increase as the shear wave speed increases.

Nanoindentation

In complex viscoelastic biological tissue, nanoindentation allows for the stiffness and elasticity of substrates of various materials to be measured locally. As with all other substrates that are subjected to nanoindentation, the objective of this characterization test is to extract the hardness and elastic modulus of the specimen being indented using a nano-scale load-displacement measurement, thus allowing for a more local measure of an area of a material when the material itself is heterogeneous. The depth of penetration beneath the specimen surface is measured

as the load is applied to the indenter. Subsequently, the known geometry of the indenter then allows the size of the area of contact to be determined [21]. The procedure also allows for the modulus of the specimen to be obtained from a measurement of the "stiffness" of the contact, that is, the rate of change of load and depth, which is the instantaneous slope of unloading when the indenter tip is displaced from the material after compression in the positive z-direction, or upwards.

Puncture Force Testing

Occluded and atherosclerotic arterial segments are hydrated, "cylindrical" in nature and are heterogeneous viscoelastic materials. This makes the samples difficult to hold in place without substantially deforming the material and altering the mechanical properties. Up until now, by attempting to mirror the crossing of a squared-tip wire through a CTO, an apparatus was built to puncture the arteries as well as other cylindrically-punched and mesh-stented surrogates axially to obtain a load versus displacement curve. However, E is not easily obtainable from these curves, there are too many unknown variables especially with respect to the boundary conditions, as the probe inherently creates a crack, which propagates in the material and complicates the data. Although the elastic modulus of fibrotic tissue is not readily obtainable by the puncture apparatus, the apparatus allows for observation of occluded artery and atherosclerotic artery behavior while under the compression force of a crossing wire. This test will become a more important test for subsequently selecting an appropriate fibrotic occlusion phantom and for guiding the creation of a fibrotic and occlusion surrogate database.

1.5 Research Objectives

The motivation of this thesis was to recommend an appropriate surrogate for fibrous tissue in CTOs to be used by SoundBite in ex vivo crossing device testing. This would help answer whether or not their technology could be used successfully in softer occlusions, specifically those that are less calcified and more fibrotic. This was to be achieved by evaluating a range of existing CTO analogs and creating new ones. A database of CTO analog properties was created to develop a suitable model for post-shockwave particle testing as well as bench testing, including performance testing, dosing studies and particle analysis.

The objectives of this research were to (i) characterize the mechanical properties of fibrotic tissue within occlusions retrieved from human cadaver femoral arteries, to be achieved by the following:

ia) defining the degree of calcification by micro-CT

ib) defining the histopathology of each sample

ic) estimating the mechanical properties from elastography

id) measuring the indentation modulus ex-vivo

ie) performing puncture tests

Subsequently, (ii) to compare mechanical properties obtained by nanoindentation and wire puncture to recommend one, or more, surrogates that can mimic the fibrotic tissue and to (iii) create a surrogate database for use by the company detailing the various mechanical behaviors of materials under the compressive force of a crossing wire. Given the small sample size of occluded arteries, a series of characterizing tests from least invasive (micro-CT) to most destructive (puncture tests) were selected to provide comparable data points between surrogates investigated.

2 Materials and Methods

2.1 Human Arterial Samples

Three donor arteries were obtained from United Tissue Network (UTN), a tissue bank located in Phoenix (AZ, United States). All were cadaveric samples and based on the donor history provided, it was hypothesized that these arteries would at least provide heterogenous plaques, stenoses and complete occlusions with fibrous tissue as a benchmark for surrogate development. Prior to beginning the study, it was not known if the arteries contained any CTOs in any of the specimens. It was also undetermined if these had important fibrotic content that would be important for future puncture force tests.

Table 1: Donor arteries used in the study

Donor Code	**Metal ID Tag**	**Label Used**	**Description**
GL1605556	A2722	Artery 2	Femoral artery - left
GL1605670	A2820	Artery 1T (Top)	Left top femoral artery
GL1695670	A2822	Artery 3B (Bottom)	Left bottom femoral artery

GL1605556-A2722 (Artery 2) came from an 87-year-old male; an avid smoker for 50 years at a rate of $\frac{1}{2}$ pack per day habit, quitting 5 years prior to death. It should be noted that the donor had triple bypass surgery in 1992 as well as a below the knee amputation on the left leg in 2016. Donor also had a gallbladder removed, a history of COPD and had poor leg circulation. Donor was not physically active and had been bedridden for 2 months prior to passing. The date of death of this donor was November 9, 2016 and the recovery date for the vessels was November 25, 2016.

GL1605670 – A2820 (Artery 1T) and – A2822 (Artery 3B) came from a 90-year-old female donor with atherosclerotic vascular disease. The donor was not a smoker, however she suffered from hypertension, poor leg circulation and had type 2 diabetes but was not using insulin. The donor had also had the pinky toe on the left foot amputated and a below the knee amputation on the right leg. Consequentially, the donor was not physically active. The date of death of this donor was December 4, 2016 and the recovery date for the vessels was December 27, 2016.

Based on the donor history provided, it was hypothesized that these arteries would at least provide heterogenous plaques, stenoses and complete occlusions with fibrous tissue for the imaging study to be relevant to the research objectives.

2.1.1 Tissue Shipping, Preservation and Storage

The arteries were requested and purchased from UTN by SoundBite Medical on April 17, 2017. These three arteries were snap frozen on the respective recovery dates mentionned above. They were express-shipped and kept on adequate quantities of dry ice during shipment to ensure that the specimens were kept frozen at -20°C. The arteries were received at SoundBite Medical on April 20, 2017 and immediately placed in a -20°C freezer. They remained in the freezer until August 8, 2017, when they were transported on dry ice to the Centre de Recherche du Centre Hospitalier de l'Université de Montréal (CRCHUM). Handling of the specimens after this point are discussed later in this section.

2.2 CRCHUM Imaging Studies

The three arteries were subjected to advanced imaging modalities to improve the understanding of the structure and characteristics of chronic total occlusions.

Starting with micro-CT, the least destructive and least intrusive modality, the full arteries were scanned, providing a complete structural picture of the arterial lumen, the occlusion(s), calcified walls, areas with calcium-embedded occlusions and stenoses. Micro-CT imaging served as the baseline arterial map for the remainder of the study, as it provided a measurement reference. Once completed, the arteries were prepared for ultrasound, where elastographic data, in the form of an estimate of E, was obtained from the full and segmented arteries. The segments were measured, frozen in optimum cutting temperature (OCT) compound with the distal end of the segment face-down (although it should have been proximal) and then sent to l'Institut de Recherche en Immunologie et en Cancerologie (IRIC) for histological slicing and analysis. The histology was deemed necessary to depict the components of the plaque, notably the fibrotic regions and provide guidance as to where to probe and cross the segments to specifically characterize fibrotic tissue in nanoindentation and puncture force testing.

2.2.1 Specimen Preparation

The three arteries were properly identified, thawed overnight and placed in Krebs-Henseleit buffer solution (Sigma-Aldrich Corp., St. Louis, MO). Before the imaging sequence began, the arteries were measured and sutured at 1 cm intervals on three sides with different colored suturing wire so as to preserve the orientation of the arteries and the eventual 1-1.5 cm segments. This color-coded orientation is shown in figure 2. Figure 3 demonstrates an artery being sutured with a strip of Fast-Find Grid (Webb Medical, Philadelphia, PA).

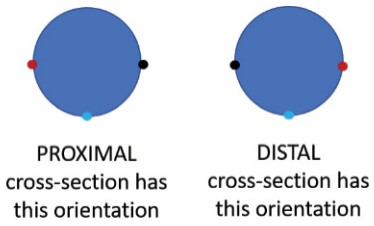

Figure 2: Marker orientation on the arterial segments for proximal and distal faces

Figure 3: Suturing of Fast-Find Grid strips to three edges of the arteries to provide orientation and distance references

2.2.2 Micro-Computed Tomography (Micro-CT)

The arteries were placed in the SkyScanner micro-CT (Bruker micro-CT, Kontich, Belgium) in a half cylinder Styrofoam insert. Figure 4 shows a visual depiction of the imaging modality and directionality. The water vial (on the left) was included in the scan for post-scan radiodensity calibration. Figure 5 shows the actual imaging stage before an arterial micro-CT scan occurred. It is important to note that the temperature inside the micro-CT was recorded at 28°C. To compensate for the heat and the dry conditions inside the scanner, damp NaCl solution-soaked gauze squares were used to cover the top portion of the arteries. Due to time sensitivity and tissue preservation, the technician opted to perform 180° scans

instead of 360° scans. The arteries were scanned for a period ranging from 45 minutes to 75 minutes. Between scans, the arteries were placed in Krebs solution and refrigerated at 4°C.

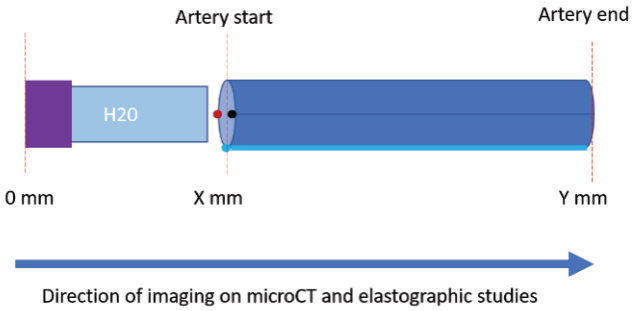

Figure 4: Schematic of the direction of scanning of the arteries for orientation purposes. The X and Y values change each artery depending on length and capturing field

Figure 5: Imaging stage of the micro-CT with Artery 1T placed in it. This image was taken prior to covering it with NaCl solution-soaked gauze

After the individual micro-CT scans were completed, the arteries were incrementally placed in Krebs-Heinseleit buffer (K3753, Sigma Aldrich, St. Louis, MO) overnight, in a circular Tupperware container, refrigerated at 4°C. The following morning, the three arteries were transported from the CRCHUM to the ultrasound facility at Hotel Dieu Hospital.

2.2.3 Elastography

All acquisitions were performed with the Aixplorer scanning system (Supersonic Imagine; Aixplorer, Aix-en-Provence, France) equipped with a 256-element linear probe (SuperLinear^{TM} SL15-4, 7.5 MHz). Dynamic elastography parameters were selected as a smoothing of 5, opacity of 50% and low acoustic power. The arteries were kept in the Tupperware containers and continually hydrated with Krebs-Heinseleit buffer while they were held stable by Aquaflex Ultrasound Gel Pads (04-02, Parker Labs, Fairfield, NJ) which were cut in half to provide two semi-circular pads. An additional gel pad was manually held on top of the artery during the scans.

Initially, the full-length arteries were scanned longitudinally and various modulus measurements of the anterior wall, the lumen and the proximal wall were taken at roughly 1 cm increments. An initial longitudinal screen capture of the system's monitor was taken to create landmarks of features of the artery, such as distinct stenoses. These longitudinal ultrasound scans would later be linked to the transversal ultrasound scans taken of each segment once cuts were made. The lengths of the segments would be used to create the link between the elastographic data obtained, the micro-CT slices (z-position) and histological slides taken of the proximal faces of the segment.

The operator used the dynamic elastography module (SSI) and adapted the power to have a complete coverage of the anterior and posterior wall. Once the colour map of elastography appeared to be stable, the image was stored and the Young moduli were measured by placing a small region of interest (ROI) respectively in the anterior, posterior wall and in the central area of the occluded vessel. For artery 2, which was not occluded, the region of interest in the lumen focused on the areas with notable stenoses and calcifications.

The arteries were segmented using a #22 scalpel following the conclusion of the longitudinal scans. Most of the segments measured at least 1.3 cm. The labelling

legend for all three arteries can be found in table 2.

Table 2: Matrix of segments made from the 3 arteries and the labelling scheme

Segment Label	**Artery 1 (A1 Prefix)**	**Artery 2 (A2 Prefix)**	**Artery 3 (A3 Prefix)**
Segment 1 (S1 Suffix)	A1S1	n/a	A3S1
Segment 2 (S2 Suffix)	A1S2	A2S2	A3S2
Segment 3 (S3 Suffix)	A1S3	A2S3	A3S3
Segment 4 (S4 Suffix)	A1S4	A2S4 (not imaged)	A3S4
Segment 5 (S5 Suffix)	A1S5	A2S5	A3S5
Segment 6 (S6 Suffix)	A1S6	A2S6 (test cut)	A3S6
Segment 7 (S7 Suffix)	A1S7	n/a	A3S7
Segment 8 (S8 Suffix)	A1S8	n/a	A3S8
Segment 9 (S9 Suffix)	A1S9	n/a	A3S9
Segment 10 (S10 Suffix)	A1S10 (test cut)	n/a	A3S10

2.2.4 Post Image Processing

After the images and sequences were obtained, the micro-CT images were analyzed on a DICOM viewer (OsiriX, Bernex, Switzerland) and correlated with the elastographic sequences, specifically the transverse images to allow for an approximate match between both types of images. These images were matched and meticulously verified by Dr. Gilles Soulez. Detailed analysis was done on each snapshot of the micro-CT scan at the segment lengths. The following data was recorded: lateral and longitudinal diameter, surface area of lumen, surface area of intimal calcium and the Houndsfield unit (HU) of the calcium, arterial walls and the lumen.

Specific analysis was done on each longitudinal and transverse elastographic snapshot at the approximate segment lengths: minimum, maximum and local average

E for the anterior, posterior walls and the lumen (some cases two luminal readings were taken) and the standard deviation (SD) of the E measurement. In the case of SSI elastography since the biological tissues examined are believed to be incompressible, $E = 3\mu$ and the algorithm to compute E assumes a purely elastic medium, where the shear wave speed can be used to obtain the E according to $E = 3\rho^* {c_s}^2$[20].

It should be noted that the HU is a commonly used quantity in CT scans (including micro-CT) to express the numbers conveniently in a standardized way. The values are obtained from a linear transformation of the measured attenuation coefficients. This transformation is based on the arbitrary definitions of air and water where the radiodensity of distilled water at standard temperature and pressure (STP) equals 0 HU and the radiodensity of air at STP is equal to -1000 HU.

2.3 Histology

Following the elastography measurements, the arteries were placed in individually-labelled vials and transported back to the CRCHUM where they were prepared for histology. The specimens were not fixed nor decalcified as the remaining unsliced segments needed to be kept intact for puncturing tests after histology. The segments were initially dried, to remove all excess liquid with gauze. The orientation colours (red, blue and black) were drawn onto the sides of the mold to be able to discern the orientation of the artery while slicing. Isopentane and dry ice were placed in a large container (glass dish) to enable the proper temperature drop. Then the cryomold was placed in the center of the container, with a few drops of Tissue-Tek OCT Compound (Catalog #: 25608-930, VWR, Radnor, PA) added in the middle of the bottom of the cryomolds.

The segments were then placed (distal face-down) in the drops and oriented in the proper direction, flat against the bottom of the mold. Additional OCT was added

into the mold until the specimen was completely covered, while leaving no tissue exposed. Excess air bubbles were removed and the OCT compound was left to settle for 15-30 seconds. The cryomolds were then frozen at -20 $^{\circ}$C, each of them covered with aluminum foil and properly labelled with a black marker according to the artery and the segment. The samples were placed into a Styrofoam box filled with ice packs and delivered to the IRIC facility for slicing and staining. For the first round of histology, two stains were used: Hematoxylin Phloxine Saffron (HPS) and Masson's Trichrome (MT). HPS differentiates between most common connective tissue, staining pink for muscle or cytoplasm and yellow for collagen. Whereas MT selectively stains muscle, collagen fibers, fibrin and erythrocytes; staining cellular tissue red, collagen and fibrous tissue as blue, cytoplasm and mucopolysaccharides or glycosaminoglycans (GAG) as light red or pink, lipids as white and cell nuclei are dark brown, black.

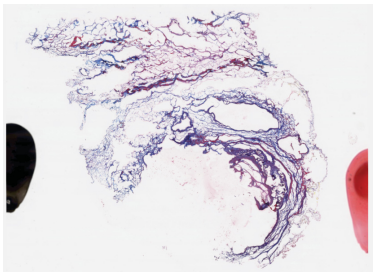

Figure 6: Histology slide obtained in the first round, illustrating the incomplete vessel slice

A second round of histology was conducted, using Masson's Trichrome and a longer stain time to darken the colors of the various tissues. The segments were also cut farther away from the proximal face to ensure that the entire cross-section would be included on the slide. The histological findings are discussed throughout the results sections.

2.4 Nanoindentation

A nanoindenting protocol was created based on a thorough literature review of nanoindenting techniques for soft tissue, hydrated materials, hydrogels and biological tissues utilizing a PB1000 mechanical tester (NANOVEA, Irvine, CA) at room temperature; The PB1000 has a theoretical effective force resolution of 0.003 µN, a maximum displacement of 250 µm in long range mode with a theoretical depth resolution of 0.03 nm. Ebenstein et al. [22] discuss methods of indenting soft biological materials with a spherical tip of diameters less than 1000 µm. Slaboch et al. [23] discuss nanoindentation of murine thrombi with a flat punch indenter. Wang's thesis [24] discusses a protocol for indenting diseased aorta tissue with a 1 mm diameter spherical tip. Ultimately, a fusion of Ebenstein and Wang's protocols was used with some guidance from the Nanovea best practices guide on indenting hydrogels [25].

2.4.1 Tip Selection

There are several tips available for the nanoindenter, however with preservation of the samples as a guiding specification, a spherical tip of 1 mm diameter was selected for the indentation of the samples as this tip is one of the more forgiving tips and has a smaller risk of creating a small crack in the arterial cross section. Although a smaller tip was initially desired, 1 mm was the smallest spherical tip that was available. Figure 7 displays a visual schematic of the tip-substance contact mechanics; R is the radius of the tip (500 µm), h_c is the contact depth, h_{max} is the maximum indent depth and r is the radius of the projected contact area of the tip with the substrate.

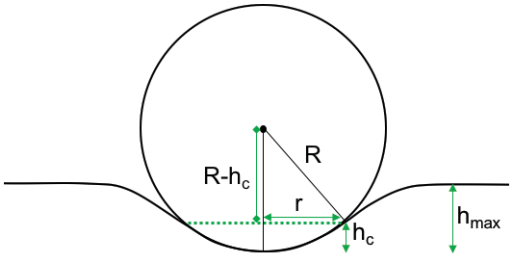

Figure 7: Contact schematic of a spherical tip with a flat surface

2.4.2 Contact Mechanics

Reduced Young's modulus (E_r), hardness (H) and unloading stiffness (S) of the arterial samples, selected gels and surrogates were calculated using the Oliver & Pharr method [26]:

$$E_r = \frac{S\sqrt{\pi}}{2\sqrt{A_p}} \tag{1}$$

Stiffness is taken as $S = \frac{dP}{dh}$ and experimentally determined as the slope of the unloading curve, where P is the force. By measuring the initial unloading stiffness and assuming that the contact area (A_p) is equal to the optically measured area of the hardness impression, the reduced modulus can be derived.

$$A_p = \pi(2r - h_c^2) \tag{2}$$

$$\frac{1}{E_r} = \frac{1-\nu_i^2}{E_i} + \frac{1-\nu_s^2}{E_s} \tag{3}$$

In (3), the ν_i and the ν_s terms represent the Poisson's ratios of the indenter and the substrate respectively. The compliance of the tip was much less than

the compliance of the samples (soft samples with $E \lesssim 1000$ kPa), therefore it is assumed that the indenter term can be neglected. It should also be noted that due to the inability to assume the value of each ν_s due to the complexity of the tissues being measured, Young's modulus in (3) was not calculated and reduced moduli were strictly used for comparison among the samples.

2.4.3 Trapezoidal Load Profile

For a viscoelastic material, the relationship between load and depth of penetration is not linearly dependent. For a given load, the resulting depth of penetration may depend on the rate of application of load as well as the magnitude of the load [21]. Thus, the indentation test is accompanied by "creep" manifesting as a change in depth for a constant applied load. For the reasons of dissipating creep, a trapezoidal load function, as shown in figure 8, was applied to the protocol in this research and consisted of a 60-70 second hold period (depending on whether depth saturation was an issue or not) and maximal forces ranged from 0.8 to 5 mN, depending on the substance being indented, was applied. The variability of maximal forces was a work around to avoid depth saturation by the mechanical tester. Loading and unloading rates were set consistently to 20 mN/min. Approach speed was consistently set to 50 µm/min.

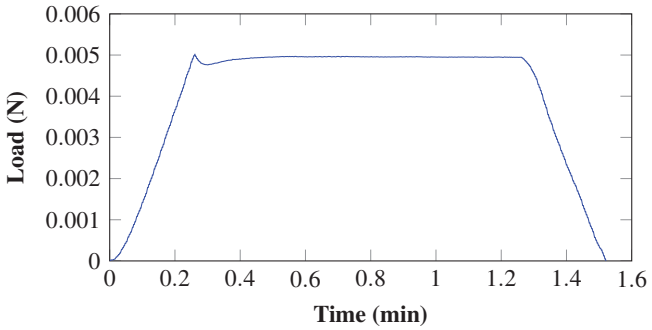

Figure 8: Trapezoidal load function applied to soft materials

2.4.4 Preparation and Indentation of Analog and Artery Samples

Agarose gels (5% w/v) were prepared using Invitrogen UltraPure Low Melting Point Agarose (Mfr. No.:16520050, Invitrogen, Carlsbad, CA) and gelatine gels (20% w/v) were prepared using type A, bloom strength 300 porcine skin-derived gelatine powder (G2500-1KG, Sigma-Aldrich, St. Louis, MO) to compare benchmark values found in Ebenstein et al.'s [22] nanoindentation study of soft hydrated materials to ensure accuracy and confidence in the method. It should be noted that the gelatine used in Ebenstein's paper was different than the type used in this research. The gelatine used in Ebenstein et al.'s work was type B bovine skin gelatine with a bloom number of 225.

Agarose was weighed (2.5 g) and mixed with 50 mL of reverse osmosis water in a flask, the mixture was stirred, however, not all the agarose was dissolved at this point. The flask was microwaved at 100% power for an initial 30 seconds, at which point the solution was removed from the microwave and swirled, then put back in the microwave for 10 second increments until the solution was completely clear. Five 60 mm diameter petri dishes were placed on the bench top and 5 mL of the 5% w/v agarose gel solution was pipetted into each petri dish. The dishes were covered, labelled and were then allowed to cool and set in a 4°C refrigerator until the gels would be needed for indentation. The remainder of the solution was stored in the flask, in the same refrigerator.

Preparation of the gelatine gels started by weighing out 10 g of the gelatine powder and mixing in 50 mL of reverse-osmosis water into a 250 mL beaker. The beaker was placed on a hot plate and constantly stirred until the gelatine was fully dissolved. Volumes of 5 mL of the solution were pipetted into five 60 mm diameter petri dishes. The gels were covered, labelled and placed in the 4°C refrigerator until they would be needed, which turned out to only be within a few days, not allowing visibly noticeable mold or bacterial cultures to grow on the surfaces.

Similarly to Ebenstein et al.'s protocol, a glass pipette with an inner diameter of 5 mm was used to press and punch samples from the parent gels, once the gels had set. The 5 mm disc samples of each gels had thicknesses of approximately 1.8 mm to 1.9 mm. The samples were only punched out of the gel as needed, as the water content of the gels would dry up if left uncovered and exposed to ambient humidity conditions. The samples were immediately placed on the glass block and fixed into place on the nanoindenter stage. The height of the indenter tip was modified to accommodate the gels and the x and y positioning was set exactly to the desired location above the gel. Due to unwanted boundary effects, 1 indent per gel was made as it is recommended to indent at spacings of approximately 5x the diameter of the indenter and this spacing was equal to 5 mm which is the diameter of the sample.

Subsequently, the remaining artery samples (12-14 samples) were tested in the nanoindenter. The frozen OCT-artery blocks were immersed in water to dissolve away the OCT and subsequently placed in Hank's Balanced Salt Solution (H6648-1L, Sigma Aldrich, St Louis, MO). They were photographed proximally and distally and areas of fibrotic tissue were verified against the histology results. The samples were secured in place by a thin layer of cyanoacrylate (or Loctite 4011 which is biocompatible) applied to the end that presents a smaller coverage of fibrotic tissue to a microscope slide as shown in figure 9.

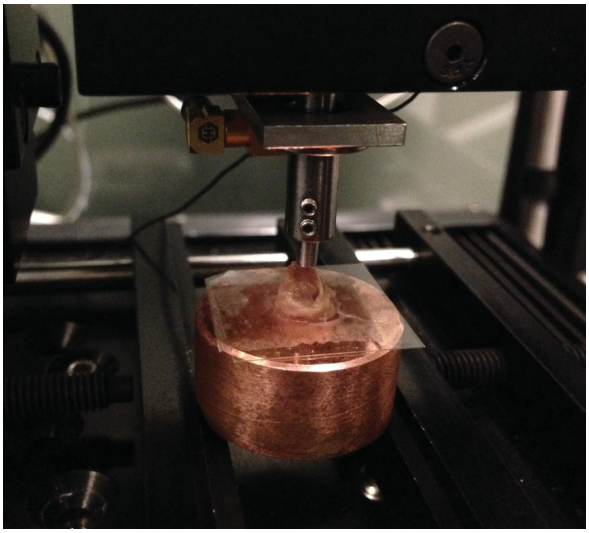

Figure 9: Indentation of an artery fragment by 1 mm diameter spherical tip, held in place on a microscope slide by a thin layer of cyanoacrylate

The samples were hydrated with some droplets of water before the indentation. The samples were placed on the stage and the indenter tip was aligned on top of the desired location, guided by the histology maps and by photographs of the proximal sample surface. Ensuring an adequate gap between the tip and the surface, the indenter load was tared. Using the software, the tip was then computer-assisted to contact the surface of the substance and lightly back off before commencing the nanoindentation. Once these preliminary steps were completed, the indentation began, and was then programmed to hold the contact load for the specified 60 or 70 seconds, provided that the piezo did not go out of range (a failure linked to depth saturation). After the pause, the indenter tip was programmed to unload at the same loading speed and go back to the starting z position. Once completed, the tip was displaced even higher, to protect against tip damage when removing the sample from the stage.

The samples with total occlusions were then frozen in individual vials containing Hanks' solution and transported back to the SoundBite lab for puncture testing. Additional dissection and nanoindenting of the arteries after the initial indenting

and puncture data has been collected will occur to further our knowledge of the local behavior and properties of the tissues in an occluded artery.

2.5 Wire Puncture Force Test

The puncture force test was performed using a Mark-10 ESM 303 motorized compression test apparatus (Mark-10, Copiague, NY) by applying a one-cycle uniaxial stress at a single velocity on the specimens until a set distance was reached. The puncture force test was performed using a penetration probe, which was designed to accommodate either a simple straight tuning wire (0.009", 0.013", 0.017") or the SoundBite™Active Wire. Puncture force tests were designed to understand the force profile and the forces necessary to cross the occlusions as well as create a more realistic specification for an occlusion surrogate. After various speeds were trialed to create a puncturing protocol, 20 mm/min was selected as the optimal speed, as the initial peak of the control material became most obvious at this speed.

To provide inter-sample puncture consistency, it was specified that all samples would measure lengths of 1-1.5 cm, since longer samples would not accommodate a realistic interventional setting where the crossing wire would be unsupported through the sample and more prone to buckling. All samples would have to be radially supported; this was achieved using a stainless steel 303, 1 cm x 2.1 cm mesh wrapped around the sample and with the overlapping edges glued together with methacrylate. Additional specifications required that the dimensions of the hole of the puncturing platform be no more than 6 mm to be representative of at most the diameter of the femoral artery. The speed of the compression jig would not exceed 25 mm/min, in accordance with ASTM F2394 6.5.4 [27]. Guided by data collected by Drs Benko and Thérasse, maximum puncture forces in excess of 2.5 N would be considered as uncrossable lesions. Lastly, the jig would have to

eventually accommodate the SoundBite Active Wire^{TM} for future crossing energy tests.

The puncture force test protocol was adapted from the ASTM F1306 standard [28], however, test parameters such as sample geometry, clamping fixture, penetration probe were changed to accommodate SoundBite's requirements specific to their application methodology.

Puncture force tests were performed at room temperature (23 $\pm$ 4°C) using a 0.013" straight and squared tip tuning wire. Samples, while punctured, were either dry or hydrated based on their handling specifications.

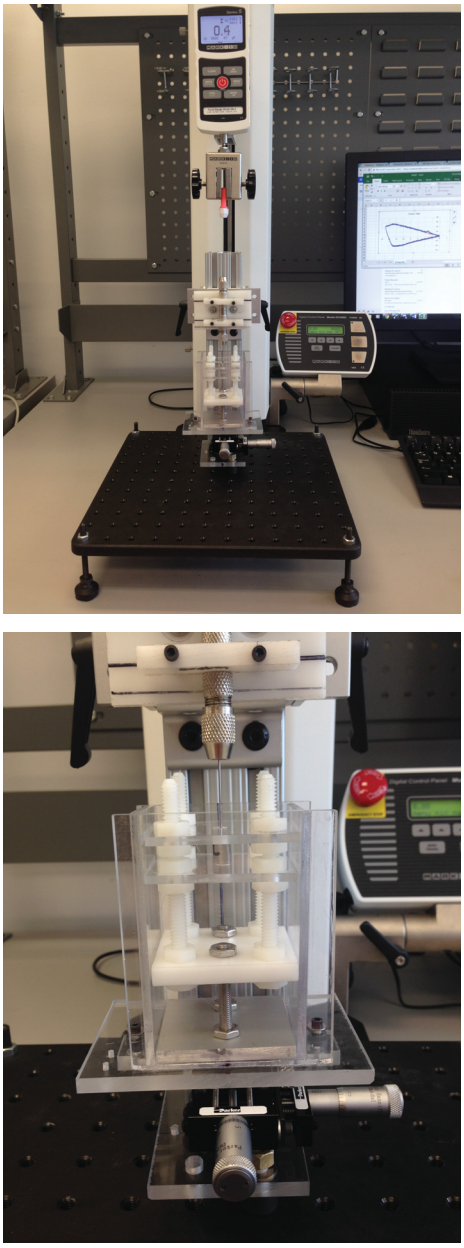

Figure 10: Custom surrogate puncture jig and sample holder

2.6 Summary of Surrogates and Tests Performed

Table 3 outlines all the mechanical tests performed on the synthetic or biological surrogates examined. Not all surrogates were subjected to both tests, this is either due to time constraints or failure to resemble the fibrotic tissue in a preliminary puncture test.

Table 3: An outline of the surrogates examined and the respective tests performed on them

Surrogate	**Class of Surrogate**	**Characterization Tests Performed**
Perma-Gel (LOCUS lab Sherbrooke University, Sherbrooke, QC)	Synthetic	Nanoindentation, puncture test
SynDaver soft (SynDaver Labs, Tampa, FL)	Synthetic	Nanoindentation, puncture test
Sausages & Pepperoni Sticks (Hot Rod - Schneiders, Great Canadian Meat Company, Jack Links; all purchased at Couche Tard, QC)	Synthetic	Puncture test
Mozarella (Ficello, Black Diamond, IGA)	Synthetic	Puncture test
Tofu (Soyganic Smoked Tofu, IGA)	Synthetic	Puncture test
Jujubes (Great Value Jujubes, Walmart, CA)	Synthetic	Puncture test
Gelatine (20%) (Sigma Aldrich, St. Louis, MO)	Synthetic	Nanoindentation, puncture of lower concentration gelatine gels
Agarose Gels (5%) (Invitrogen, Carlsbad, CA)	Synthetic	Nanoindentation
Ginger (store bough at IGA)	Synthetic	Nanoindentation
Glutarhydrate-fixed bovine pericardium (Leask Lab McGill University, Montreal, QC)	Biological	Puncture test
Chicken skin (peeled off store-bought chicken breasts at IGA)	Biological	Puncture test

3 Results

3.1 Arterial CTO Structure and Composition

Micro-CT images were captured for all three arteries. In figure 11, micro-CT slides juxtaposed with histology slides of notable sections of artery 1 are displayed. Artery 1 was visibly occluded for 85% of the length of the specimen, until segment 8 (A1S8) where a small dark circle appears, indicating an aperture in the occlusion. Artery 3 was completely occluded for the entire length of the specimen. Artery 2 did not show any regions of complete occlusion; however, it was extensively calcified and had three regions of moderate to severe stenosis, for this reason, along with the method in which we segmented the artery, the results will mostly be focused on arteries 1 and 3. For detailed notes on the micro-CT scans refer to table 8, found in the appendix section. For micro-CT snapshots of arteries 1 and 3, see figures 26 and 27, also found in the appendix section.

Although the micro-CT imaging of each artery represents a catalogue of cross-sectional slices that span the entire length of the artery, the histology slides needed to be juxtaposed with the micro-CT slices. The micro-CT slices were assigned a z-position (location) based on features and wall shape that were found in elastography as well as the length of the individual segments. The histological slides were linked to the elastographic transversal scans as they represent the distal face of each arterial segment and from this a position could be given to the histology slides. These elastographic values juxtaposed with the histology findings are presented in table 4. This ultimately lead to reconstituting the mechanical characteristics of the entire occlusion and provided a histological map outlining, specifically, the fibrotic regions.

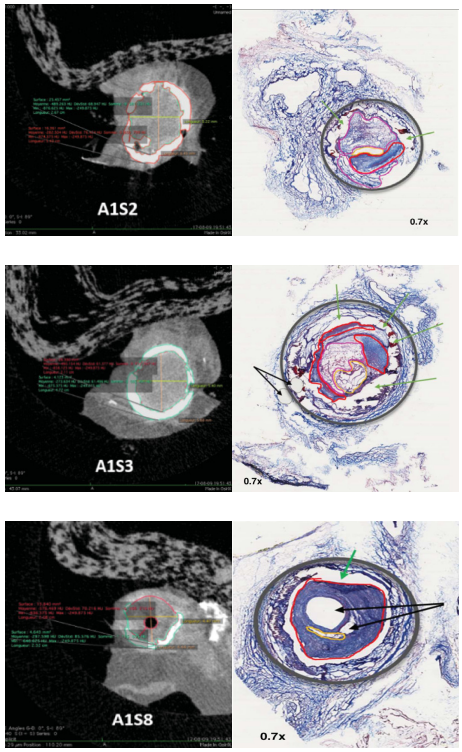

Figure 11: Micro-CT static images and histology slides for A1S2, A1S3 and A1S8 segments. The red area indicates dense fibrous tissue and the pink areas indicate looser, less organized fibrous tissue. The yellow area represents lipid accumulations or cholesterol clefts. The green arrow points to calcified regions, the black arrows indicate apertures or artefacts in the occlusions.

Most of the histology analysis served as outlining regions of suitable indentation and puncture for characterizing fibrotic tissue, as well as highlighting other regions that could provide interesting characterization results; for this study, the regions that were be punctured are those in red and pink. Because only some histology slides remained intact, the ones that were damaged by the intimal calcium had to be macroscopically observed and regions of fibrotic tissue (if any) had to be inferred before puncture based on the resemblance to other fibrotic regions found on the segments with an intact histology slide. From histology it was confirmed that there was fibrotic content (loose, medium or densely organized) present in

each of the slides analyzed. Whether the fibrotic content was small or large, the magnification of these specific sections revealed common patterns of deposition and formation. The denser the fibrotic tissue, the more organized and layered it appeared. See figure 12 for the layering structure repeatedly observed in arterial occlusion-dense fibrotic tissue; the tissue of interest is stained blue.

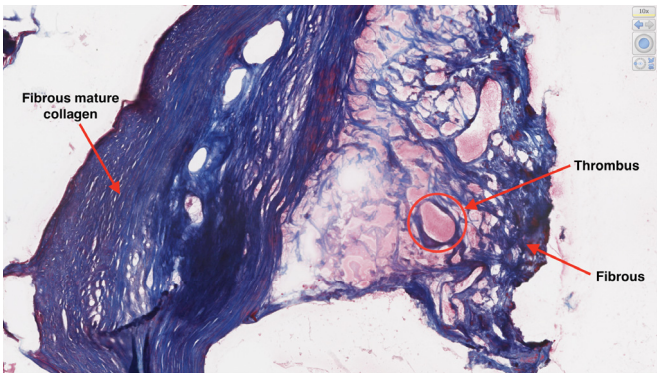

Figure 12: 10x magnification of MT-stained dense fibrotic tissue and thrombus

3.2 Elastography

In this section, closer examination of the elastic moduli is conducted and juxtaposed against the findings of elastic values and their SD. Although E values, measured by elastography, where measured in the middle of the segments (due to the nature of ultrasound and to maximize the quality of the measurement of the segment) and histological slides corresponded to the distal face of the segment, they did not correspond to the exact z-position however, in tandem, the results may lead to more substantial findings. Elastography has not yet been proven as a precise measurement method of E of the anterior, posterior walls or lumen in atherosclerotic or completely occluded arteries. However, alongside the E, the SD of the elastic modulus obtained is an important value as it provides insight into the region's homogeneity or heterogeneity. If the standard deviation is $>10\%$ of the mean modulus measurement in the anterior wall, luminal or posterior wall,

the region is considered to be of heterogeneous composition. The luminal heterogeneity was also further confirmed by cross-examining the histological slide that corresponded to the transversal scan. On the slides with damaged tissue, it was impossible to confirm this. However, on the slides that remained intact, the SD did provide correct predictions of regional composition. Table 4 juxtaposes the elastic modulus measurement of the lumen (usually exactly in the central portion of the luminal cross-section), the SD, the histological findings as well as the prediction of homogeneity or heterogeneity of the lumen as indicated by the SD. Very few arterial cross sections are of homogenous composition, notably only one kind of fibrous tissue or organization, but the homogenous value could be used as kind of a "standard" E value for that specific tissue. These were the values that were used for comparison in the puncture and fibrotic characterization tests of the arterial segments. The elastic values in the more distal portion of the arteries (both A1 and A3) seemed to match the subsequent histological slide. Seeing as the measurement taken via elastography was central as opposed to distal, this is a very likely explanation of the phenomenon observed. From elastographic measurements of arteries 1 and 3, it was postulated that the appropriate range of the E for fibrotic tissue in a lumen is likely 33.6 - 44.2 kPa. Due to the relative novelty of using this technique on occluded arteries, no similar values were found in the literature to compare the obtained values with.

Table 4: Correlation of E and SD with plaque composition and histological findings for artery 1

Segment	**E (kPa)**	**SD**	**Predicted Composition**	**Elastic-Histological Findings**
A1S1	36.5	3.7	Homogenous	Mean luminal elastic value suggests fibrous, lower SD means it's mostly fibrous. Histology shows damaged slide, however the intact regions are densely packed fibrous tissue
A1S2	5.4	3.8	Heterogenous	Lower luminal elastic value could suggest a very loose thrombus, however lots of calcium in the vessel walls.
A1S3	10	6.8	Heterogenous	Highly heterogenous with sections of loose fibrothrombotic tissue as well as a specific section that is densely fibrous
A1S4	1.4	1.3	Homogenous	Very calcified, micro-CT suggests calcified, correlation elasto is impossible (most of the signal in the lumen is artifacted by air or liquid)
A1S5	27	7.1	Heterogenous	Might correspond to A1S6, as histology shows a lumen that is more thrombotic, less mature and less organized (soft)
A1S6	40.5	13.5	Heterogenous	Histology shows a varied lumen with two striated layers of medium packed fibrous tissue that surround a more liquid/thrombotic region
A1S7	40.8	10.7	Heterogenous	Fibrous, large SD value suggesting the fibrous and other component heterogeneity
A1S8	34.9	9.7	Heterogenous	Layered fibrous tissue, regions of medium density separated by thin layers of denser fibrotic tissue
A1S9	8.9	8.4	Heterogenous	Dense fibrotic regions found in histological analysis however the elastic value is lower than expected most likely due to air (non-occluded portion of the artery) that is lowering the signal

Overlaying the micro-CT densities (measured in HU) and the elastography-measured E of the luminal region and the anterior wall of the arterial segments does not necessarily provide adequate explanations as to why E would be lower than expected in a fibrous lumen (as confirmed by histology). There could be human measurement error linked to the large size of the selection field of the elastographic instrument on the screen compared to the selectable cross-sectional surface area of

the arterial segment. However, secondary measurements were taken of the lumen on a few segments and tracked within the error range of the primary measurement. Upon closer observation, A1 had significantly lower wall density values (on micro-CT) then did A3. The walls in A1 had an average value of 305.23 HU, the walls of A3 had an average value of 1375.34 HU. The walls of A3 were presumably denser than that of A1 and referring to the known density values found on CT scans (see Table 5), the A3 walls could have been closer in composition to cancellous bone, thus structurally stiffer.

Table 5: Known density values found on CT scans

Substance	**HU**
Air	−1000
Fat	−120 to −90
Soft Tissue, Contrast	+100 to +300
Bone	+200 (craniofacial bone)
	+700 (cancellous bone)
	+ 700 to +3000 (cortical bone)
Water	0
Blood	+13 to +50
Clotted Blood	+50 to +75
Muscle	+35 to +55

3.3 Nanoindentation

Table 6 lists the reduced modulus and standard deviation for the A1 and A3 medium-loose to dense fibrotic unpunctured arterial samples, 5% agarose gels, 20% type A porcine gelatine gels, Perma-Gel, ginger and SynDaver samples. Figure 13 visibly compares the values of the materials indented, without the inclusion of 5% agarose and the ginger in order to provide a clearer comparison of similar scales of magnitude.

Table 6: Nanoindentation-derived reduced elastic modulus of various substrates including the unpunctured arterial samples

Substance	E_r(kPa)	SD	# of Samples
Dense Fibrotic Tissue	52	17.1	9
Medium Fibrotic Tissue	23	5.0	13
Med-Loose Fibrotic Tissue	14	1	3
5% Agarose	406	29.2	9
20% Type A Porcine Gelatine	101	11.6	4
Perma-Gel	69	10.5	4
Ginger	387	31.9	2
SynDaver Soft	38	n/a	1

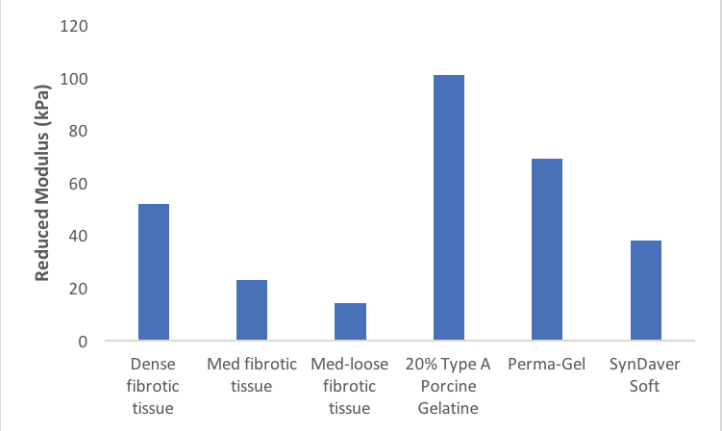

Figure 13: Graphical comparison of the nanoindented materials' reduced moduli, not included are the 5% agarose and the ginger samples

3.3.1 Indenting Control Material

The reduced modulus for 5% agarose was found to be 406 ± 29.2 kPa after 9 sample indentations whereas the reduced modulus for 20% type A porcine gelatine was 101 ± 11.6 kPa after 4 sample indentations. Ebenstein et al. [22] obtained a reduced modulus of 0.84 ± 0.04 MPa for 5% agarose which is about twice the values obtained for these two types of gels in this research. Although they used a

similar trapezoidal load indenting protocol, there were notable differences between both experimental setups such as the length of hold at the peak load; Ebenstein et al. applied a 5 second hold compared to the 60-70 second hold time, their use of a smaller spherical indenter tip, 100 µm diameter as compared to 1000 µm diameter tip, the gelatine they used was from a different animal source as well as had a lower bloom strength. Lastly, there are possible batch variances in making both gels as well as the method of calculating the unloading slope $\frac{dP}{dh}$, which was not mentioned in their paper. Nonetheless, for the purposes of this thesis, the values obtained for agarose and gelatine were repeatable and deemed acceptable and were within a wide range of several other reduced moduli found in the literature.

3.3.2 Arteries

Using the histology as a guide and the degree of layering within the blue-stained (collagen) tissue, the reduced moduli of fibrotic tissue was categorized into three categories: dense, medium and medium-loose. The reduced moduli of these tissue types were 52 $\pm$ 17.1 kPa, 23 $\pm$ 5 kPa and 14 $\pm$ 1 kPa respectively. The modulus decreased as the density, or degree of organization, of the fibrotic tissue decreased. With various attempts at modifying the quasi-static indentation protocol and the 1mm indenter tip, it was not possible to obtain any notable results for loose fibrotic tissue or thrombus, as the indenter would go "out of range" during the 70 second pause, unable to hold the load for the full duration.

3.3.3 Synthetic Surrogates

The SynDaver soft samples were extremely soft and hydrated and proved difficult to obtain a full indentation test without the piezo sensor going out of range,

similarly to the looser fibrotic tissue samples. With regards to the other substances indented, the reduced modulus of Perma-Gel was found to be 69 ± 10.5 kPa, a little too high compared to the fibrotic tissues. The SynDaver soft occlusion material provided the most comparable reduced modulus to the fibrotic tissue. However, the fact that only one sample indentation of many provided a suitable unloading curve to calculate the reduced modulus, undermines the strength of this comparison.

3.3.4 Biological Surrogates

Due to a lack of time and late surrogate discovery, no biological surrogates were indented.

3.4 Wire Puncture Force Test

3.4.1 Puncture Control Material

Perma-Gel, a nonaqueous gel composed of a proprietary blend of a styrenic block copolymer and an oil [29], touts having similar mechanical properties as gelatine ballistic gel of 10% however, being nonaqueous, it is solid at room temperature, not subject to bacterial growth and easily reusable and remoldable into any shape or size. Perma-Gel was readily available in the SoundBite Medical labs and meets many of the characteristics for the "ideal" surrogate material.

Upon puncturing the 1 cm long, 0.6 cm diameter, stainless steel mesh-stented samples of Perma-Gel it was adopted as the "control" material for verifying jig positioning, alignment and degree of kinking of the metallic guide tube. At the 20 mm/min speed, similar to the ASTM F1306-16 [28] standard, there were two

characteristic peaks consistently visible: the initial boundary puncture and the full length puncture of the sample by the wire. This curve was obtained consistently, demonstrating the pushing friction associated with the material between the initial and final puncture and the pulling friction when the wire was being removed from the sample.

3.4.2 Arteries

All punctures of the arterial samples were targeting fibrotic tissue found on the surface of the arterial sample and embedded into the occlusion plaque. As such, there was a repeatable characteristic curve observed for crossing these tough fibrous tissues. The curve resembled that of a parabolic curve, if not quartic followed by one or two sharp drop-offs in load. After this initial puncture of the fibrous material, it was difficult to conclude which tissues were subsequently punctured as the wires rarely held a straight trajectory through the samples and sometimes (usually) deflected into the intimal space as the wires tend to take the path of least resistance when being pushed at a constant speed. However, regardless of the path, a high degree of heterogeneity was consistently observed.

This characteristic portion of the curve is demonstrated in figure 14a. The peak load achieved right before rupture varies depending on thickness of the fibrotic tissue, the degree of organization as well as whether there is local heterogeneity surrounding the punctured region. For instance, looking at figure 14b, A1S4 appears to be quite similar to A1S5, however, upon observing the distal face of the segment, A1S5 is still completely occluded whereas A1S4 has a significant luminal void. The fibrotic tissue observed in A1S4 is not thick enough to provide a similar peak load seen in A1S5 and A1S6.

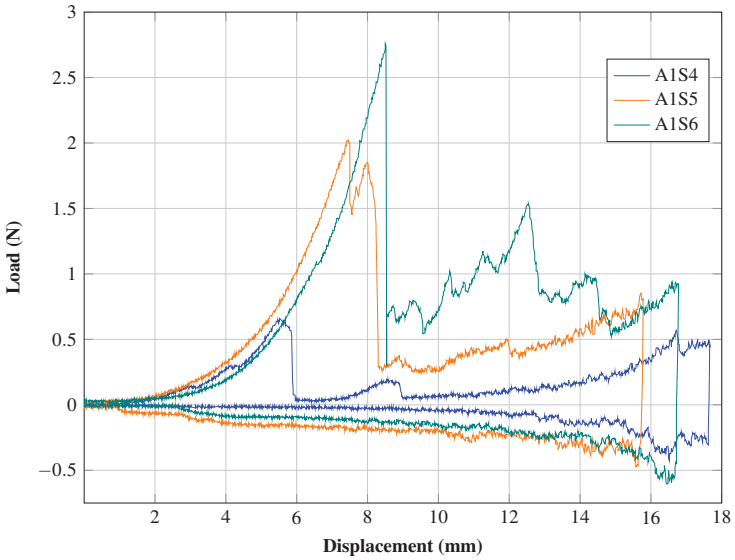

(a) A1 segment puncture curves for fibrotic and fibrothrombotic tissue punctures

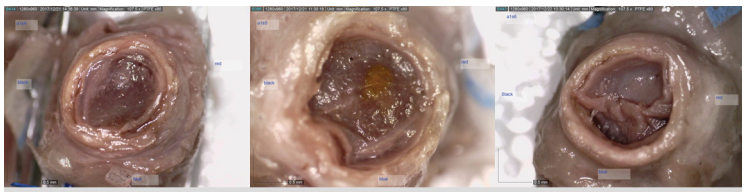

(b) A1S4, A1S5, A1S6 proximal faces pre-puncture

Figure 14: Juxtaposition of puncturing curves with arterial cross-sections prior to puncture

It should be noted that the occluded artery 1 contained much looser fibrotic tissue compared to artery 3, where almost no fibrotic samples were successfully punctured without the wire buckling. Interestingly, the samples that were crossable were not indentable and vice versa. There were no arterial samples that were both indented and punctured. Almost all the artery 3 samples were not crossable via the puncture test.

The initial, non-linear curves for fibrotic tissue punctures were isolated and analyzed in more detail to help with material comparisons. Both these specimens

appear to be displaying a hyperelastic response, that of a strain hardening material.

3.5 Synthetic Surrogate Database

A synthetic surrogate database was created of all the synthetic surrogates examined for their potential to mimic the behaviors of fibrotic tissue found in CTOs while punctured; this would be the most relevant test for the device. Some of these materials were indented, however, as will be discussed later in section 4, the reduced modulus of the indented substrate didn't necessarily translate to being a representative surrogate material for puncturing fibrotic tissue. Seven potential synthetic surrogates were examined: Perma-Gel, various concentrations (% w/v) of gelatine, jujubes, mozzarella, extra firm tofu, SynDaver soft occlusion models and SynDaver hard occlusion models. The notable specimens are discussed below and a summary of all the surrogate results can be found in the appendix, in table 11.

3.5.1 Perma-Gel

Figure 15 demonstrates the characteristic wire puncture load-displacement curve of Perma-Gel at 20 mm/min with a 0.013" wire. This material serves as a great puncture force test control material, as it displays the same curve every time it is punctured. Unfortunately, this material is not resistant enough to puncture and compared with the arterial samples, Perma-Gel displays higher wire-tissue friction and lower peak loads.

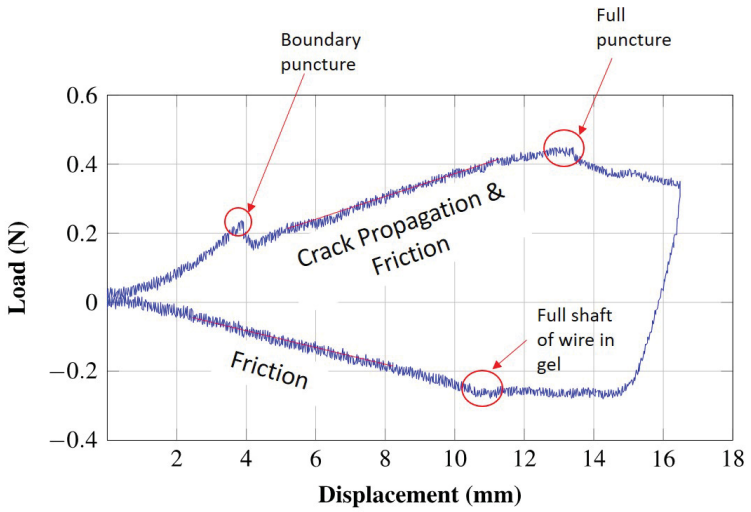

Figure 15: Permagel load displacement curve with a 0.013" tuning wire

3.5.2 SynDaver Soft Occlusion

Marketed as an adequate surrogate for a soft CTO, this material showcases the similar properties of a gel; most likely a hydrogel, where it gains structural stiffness when the polymer network is hydrated and swollen. It was observed, in experiments carried out in this thesis, that the wire puncture load-displacement curves, seen in figure 16, of SynDaver soft occlusions are not adequate representations of a fibrous CTO and are more similar to that of the Perma-Gel, only marginally stiffer. An initial boundary peak is observed as well as a complete sample puncture. There is greater frictional resistance between the initial peak and the final peak compared to Perma-Gel and compared to the arterial samples. Once the complete puncture is obtained, a sharper decrease in load is observed than that of the Perma-Gel, since the wire creates, similarly to the arterial sample, a wide channel. This burrowing is further evidenced by the lack of frictional resistance (near zero load) when the wire is pulled out of the sample.

It is important to note that the peak loads while crossing the soft SynDaver occlusion are lower than the arterial samples (1N versus greater than 2N).

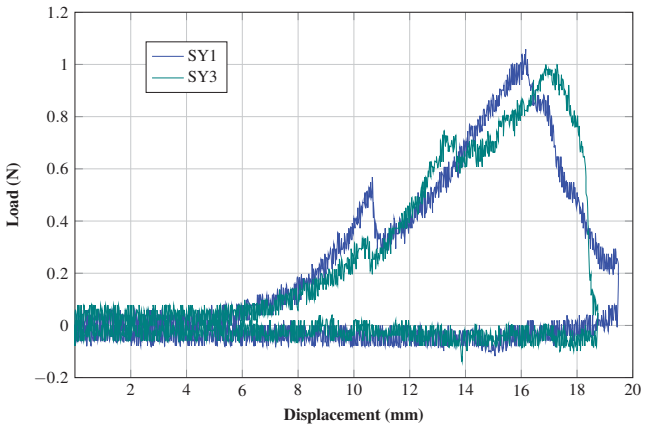

Figure 16: SynDaver load displacement curve with a 0.013" tuning wire

3.6 Biological Surrogate Database

Similarly to the synthetic database, a biological surrogate database was compiled for their potential to mimic the behaviors of fibrotic tissue found in CTOs while punctured. These materials were not indented as their similarity to fibrotic tissue was only discovered after the puncture tests. Three biological surrogates were examined: glutarhydrate-fixed bovine pericardium, chicken skin and a variety of pepperoni sticks and dried sausages. All three specimens are discussed below and a summary of all the surrogate results can be found in the appendix, in table 11.

3.6.1 Bovine Pericardium

The pericardium is a thin double-layer sac which encloses the heart protecting it within the chest cavity. It is made up of three membranes, but of most relevance to finding a fibrotic tissue surrogate is the fibrous membrane. This is the outer-most layer and is dense connective tissue composed of collagen and a few elastin fibers. Several samples of this tissue were available in the Leask Lab from Tiffany

Zigras' [30] thesis. The tissue had been fixed in glutarhydrate and some untested samples had been left in cassettes. Compared to the fibrotic tissue in the arteries punctured, a similar non-linear loading profile followed by a sharp drop-off in load is observed in the layers of bovine pericardium punctured. The most similar peak load to that of the arterial fibrotic tissue is obtained with a two layer puncture as shown below in figure 17.

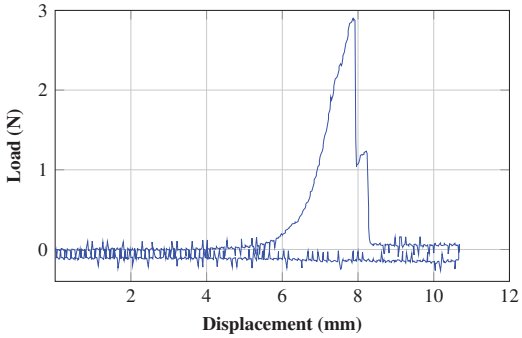

Figure 17: Load-displacement curve for a two layer sample of fixed bovine pericardium

Because the pericardium was a sheet-like surrogate, as shown below in figure 18, it was not punctureable with the puncture jig described in the materials and methods section and a work-around solution for holding the sample was used. The sheets were clamped down tightly by two plates with a central 7 mm aperture to allow for complete puncturing without the sample caving in and slipping out of the hold. This was not a perfect work-around as no measurement was taken of how much force was required to securely tighten down the sample. It is hypothesized that the clamp-down force for a sheet-surrogate would affect the results obtained, mostly the peak load. However, the loading curve was unchanged with clamping tightness, only the peak load was affected.

Figure 18: Single layer of glutarhydrate-fixed bovine pericardium

The curves obtained from puncturing pericardium were of the shape and in the magnitude ballpark for peak load and rupture. Shown below in figure 19 is the similar hyperelastic puncture curves found of bovine pericardium and fibrotic tissue of A3S10. Although the peak load of the pericardium is slightly lower than that of the fibrotic tissue, the peak load of the pericardium is still within range of all the fibrotic tissue punctured. What is interesting is the same two-tiered drop off in load that occurs in both substances as this effect wasn't always observed in the less dense fibrotic tissue rupture.

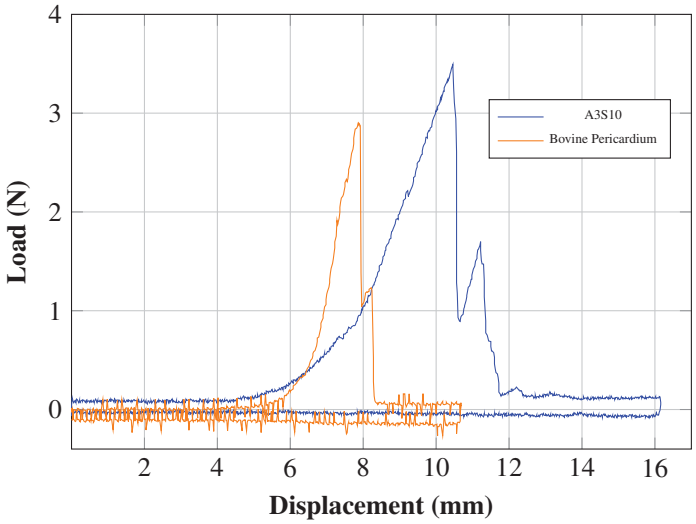

Figure 19: Juxtaposition of similar load-displacement curves of double-layered pericardium and fibrotic tissue in A3S10

3.6.2 Chicken Skin

Since bovine pericardium is not the easiest tissue to procure, another promising solution is using chicken skin, as shown in figure 20. It's a viscoelastic material that contains approximately 75% type I and 15% type III collagens [31]. Similarly to bovine pericardium, chicken skin, can be layered to simulate higher loads comparable for crossing thicker or denser fibrotic tissues.

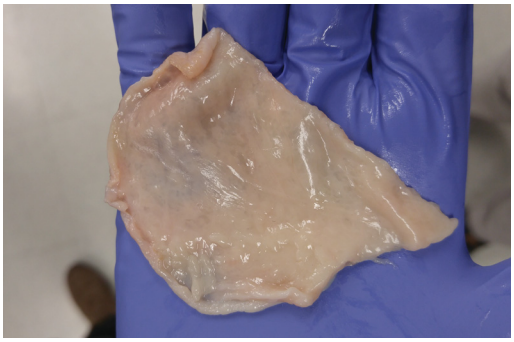

Figure 20: Single layer of chicken skin freshly harvested off a chicken breast pre-puncture

Figure 21 illustrates is a characteristic fibrotic tissue curve which is a hyperelastic response under load, followed by an immediate drop-off in load obtained from puncturing a single layer of chicken skin as well as the results from puncturing a two-layered sheet, where the loads increased to peak values of 2.4 N for the top layer and 2.9 N for the bottom layer. Puncturing multiple layers of chicken skin is promising, but the holding method needs refinement; the curve shown in *b* shows a middle peak, postulated to be a fold in the bottom layer. Chicken skin provided highly relevant preliminary results and is more cost effective and a more readily available surrogate than bovine pericardium.

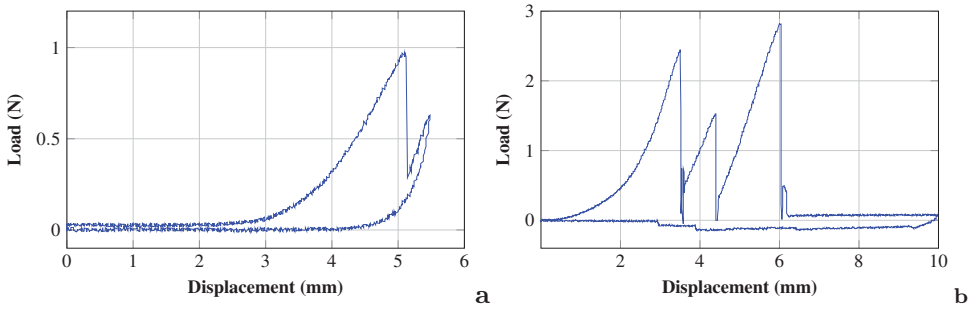

Figure 21: Load-displacement curve of (**a**) a single 2mm layer and (**b**) 2 layers of 2 mm thick chicken skin

3.6.3 Sausage and Pepperoni Sticks

Sausages or commonly purchased pepperoni sticks exhibit sample to sample variability; there is a substantial degree of heterogeneity when they are punctured as shown in figure 22. Periodically, a puncture of a pepperoni, notably in the Jack Links Wild variety, will demonstrate similar peak loads (barely over 2N) as arterial punctures. However, out of the numerous samples of pepperoni punctured, this was an outlier. Sausages are better surrogates for crossing a heterogeneous substance however they inconsistently meet the stiffness criteria and fail to exhibit the sharp drop-offs in load. They are manufactured by a grinding and blending process rather than matrixed together. This means that they are more porous than an occlusion, oily (lubricated) and thus easier to cross.

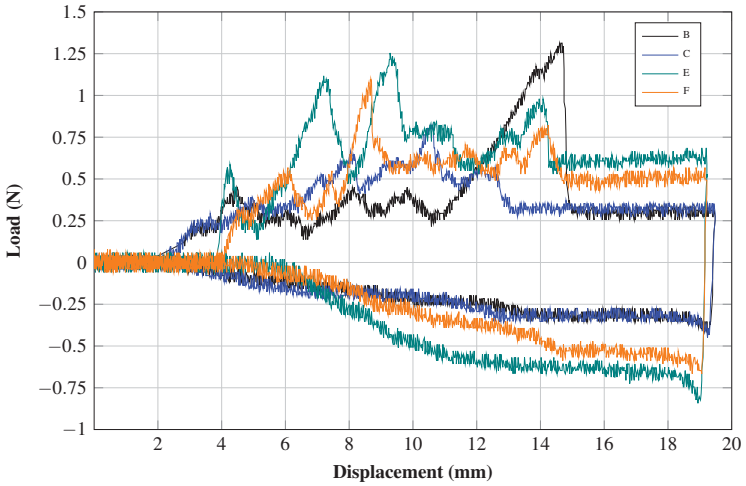

Figure 22: Load-displacement curves of 4 samples labelled as B, C, E, F of Schneiders Hot rod pepperoni obtained with a 0.013" tuning wire

The very mechanism that makes the sausages heterogeneous also introduces an unknown batch variability factor which is simultaneously a deterrent and an ideal property of this surrogate material. A perfect complete occlusion surrogate would be a stiffer pepperoni, and exhibit higher peak loads. However, when considering

pepperoni as an adequate surrogate for fibrotic tissue, it doesn't exhibit any exponential loading or any major elastic deformation under compression, making it an unsuitable fibrotic surrogate.

4 Discussion

The purpose of this thesis was to investigate and characterize fibrotic tissue in CTOs and to propose potential fibrotic surrogates for SoundBite Medical and their novel percutaneous intervention crossing device. Characterization results of all materials were obtained from least-invasive to most invasive, in order to preserve the limited samples as long as possible. Studies began with the imaging suite: micro-CT scans, elastography, histology, followed by nanoindentation and concluded with puncture tests. After the analysis of the results, all studies were found to be somewhat complementary and provided another piece of the fibrotic puzzle. There were definite relationships observed between the density of the fibrous tissue, degree of organization and the reduced modulus from the indentation testing: the denser the fibrous tissue and more organized, the higher the reduced modulus. Interestingly, although the reduced modulus of some of the analogs was similar to the fibrotic tissue, those particular materials did not produce similar wire penetration load-displacement curves. Additionally, the materials that were indentable, thus hard enough, were not crossed successfully in the puncture tests, causing the wire to buckle or permanently deform.

The results provided the company with ample evidence that fibrous tissue, although not as hard as calcium, is not a simple visco-elastic structure to cross and can sometimes be the hidden reason for wire deflection into the sub-intimal space or even as failures in percutaneous interventions. Depending on thickness, density or strength of attachment to the surrounding substrates in the plaque or on the vessel wall, the amount of force needed to cross a fibrotic tissue can easily exceed the forces typically exerted by the interventionist pushing on the wire, which is roughly on the order of 2-2.5 N.

Considering the composition of fibrotic tissue, it is was not surprising to have repeatedly observed the resilience to puncture and the higher-than-expected mechanical strength of this type of tissue. As a connective tissue, there are several

important molecules that allow fibrotic tissue to generate different mechanical properties. In general, these molecules either resist tensile and stretching forces or compressing forces. Collagen is the main component that resists deformation. Elastin also resists deformation but behaves similar to rubber in that it can be stretched and will recoil after the force is removed [32]. Another constituent is the family of glycosaminoglycans that resist compressive forces, specifically hyaluronan, which is an important compression-resisting component of connective tissue. Given this, it would make sense for a non-linear load increase to occur when attempting to puncture the fibrotic tissue embedded within the occlusion.

4.1 Puncture Mechanisms

Not all occlusions are alike, however, fibrotic tissue embedded in occlusions were observed to rupture consistently in similar ways. Typically the wall was completely calcified or very hard and the tissue was extensively anchored to the entire length of the wall. Due to the viscoelastic nature of the fibrotic structure, the instant a compressive force was exerted on the occlusion, the whole structure would cave in on itself. This behavior sets it apart from the gels investigated, since the gel structures remained intact after puncture. This elastic rupture effect is highlighted in figure 23, showcasing the proximal pre and post-puncture structures of A1S6.

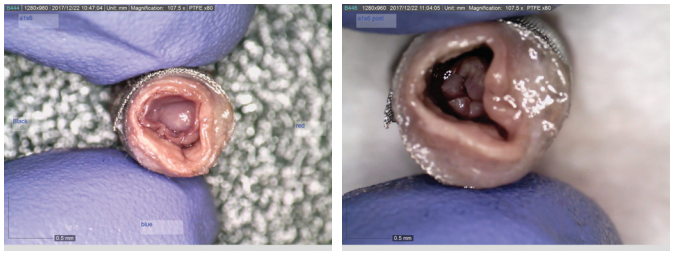

Figure 23: Proximal images of A1S6 pre-puncture (left) and post-puncture (right)

The initial exponential puncture curve characteristic of fibrotic tissue comes from the connective tissue components reorganizing themselves under compression and tension generated by the wire. Once the puncture has been made, there is an absence of recoil in the tissue, so the wire is simply cutting the now-inelastic tissue pushing the ruptured fragment of fibrotic tissue downwards through the remainder of the occlusion. Additionally, the post-puncture load-displacement fluctuations are likely caused by further tearing of the connective tissue from the hardened walls of the artery. This effect was seen in most fibrous-occluded arteries and, just as in figure 23, it is shown again in figure 24, where histology depicts A3S3 as having a medium-dense fibrotic occlusion surrounded by a calcified wall and where post-puncture, the walls are clearly shed of fibrotic tissue and the wire has created a fibrotic cluster at the distal end of the artery with a channel indicating where the wire passed through.

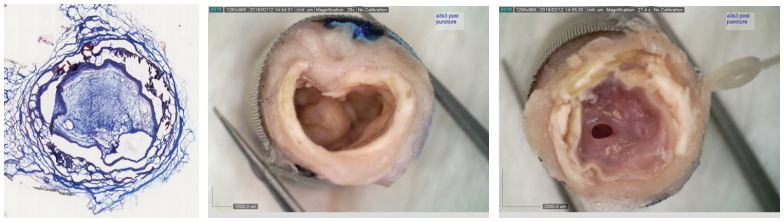

Figure 24: MT-stained A3S3 (left) juxtaposed with post-puncture images of A3S3 proximal (center) and A3S3 distal (right)

Although this thesis didn't examine the creation of particulates following puncture of the fibrotic tissue, it is hypothesized that fibrotic tissue, when punctured, can create or dislodge particulate matter. Figure 25 shows a fragment of fibrotic tissue obtained from puncturing the A1S4 sample in the wire puncture force test.

Figure 25: Fragment of fibrotic tissue in A1S4 created from puncturing via a 0.013" straight tuning wire

4.2 Nanoindentation and Puncture Force Values

Several samples were indented to obtain local reduced moduli to compare the specimens to the fibrotic tissue. Most of the potential surrogates had higher than expected E_r, obscuring the likelihood that any of these materials would provide adequate surrogates. If the E_r had been the only measurement used to correlate similar materials and mechanical behavior, the wrong materials would have been suggested as surrogates. For instance, the two surrogates with E_r values and the artery samples (SynDaver soft with an E_r of 38 kPa and Perma-Gel with an E_r of 69 ± 10.5 kPa) were shown to be inadequate when punctured, exhibiting lower initial boundary rupture forces and lacking an instantaneous, near-zero load drop after this initial puncture. Additionally, the wire-substance friction in these gels were much higher than the fibrotic tissue.

Due to time constraints, pericardium and chicken skin were not indented. These biological surrogates would likely provide higher values because both materials are more organized, but they would have to be tested to confirm this hypothesis. Regardless, based on the importance of the puncture test results and the test's relevance to the clinical setting, it is still recommended to use a fibrous biological

material such as pericardium or chicken skin for SoundBite Medical to test their device; no gels tested ever failed the puncture tests, whereas the fibrous sheets caused wire buckling on some trial runs.

4.3 Correlating the Measured Elastic Moduli of Fibrotic Tissue

Closer examination of elastographic and micro-CT data could explain some of the discrepancies observed for the E values obtained in varying densities of fibrotic tissue. One of the quantities measured in post-micro-CT analysis was the thickness of the calcified walls and the light density of the walls and luminal regions. Although higher E values were expected in artery 3 than in artery 1, the micro-CT data shows that artery 3 had a much denser, stronger bone structure and could be a factor in how much of the ultrasound wave was able to penetrate the walls or if the walls in A3 obscured the measurements taken in the lumen. The luminal values (micro-CT) for A1 averaged 22.82 HU whereas A3, which was more than A1 according to histological findings and visual confirmation, averaged at 12.76 HU. Looking at the wall thicknesses of A1 in Figure 26, and comparing them to figure 27 (both found in the appendix), the walls look and measure out to be thicker in A1. However, if they are different types of bone or bone-like calcific structures, then this would explain why the walls of A3 are thinner, more dense and more resistant to the elastographic measurement of the lumen, effectively providing an explanation of the lower values if true. A summary of transverse results obtained by elastography is presented in figure 28, in the appendix. These values were collected by Dr. Soulez and plotted according to the region he classified them as: anterior wall, thrombus, vessel interior, stenosis, posterior wall. There could have been some overlap between values in the thrombus group and the vessel interior group as it was difficult to conclude this specific information purely based on the ultrasound monitor. There is a slight decrease in the elastic modulus

values obtained from longitudinal measurements compared to the values in the transversal scan. This is interesting as it could be related to the fragmentation of the calcium in the walls upon segmentation, providing less structural reinforcement. But this can also be related to the shortened length of the segment. A larger sample size of arteries would be needed to confirm these hypotheses. Interestingly, the elastographic-measured E of fibrotic tissue ranged from 33.6 to 44.2 kPa. Although this is a general hypothesis pertaining to a non-categorized type of fibrotic tissue, pooled together, the mean reduced moduli of the all the arterial samples indented was 33 $\pm$ 18.5 kPa (a relatively high SD). A direct conclusion cannot be made as to whether or not the elastography values are indeed correct, since the elastography predicts E rather than the E_r. Due to the heterogeneity of the plaque and of the fibrotic tissues themselves, it was not accurate to assume a Poisson's ratio of 0.3 for these indentations and for that reason, the reduced modulus was calculated and simply used as a basis for comparison amongst the other types of surrogates.

4.4 Surrogate Database & Recommended Surrogate(s)

In table 7, the surrogate database is shown. This table compiles all the quantitative and mechanical properties collected for each surrogate tested. Some materials had comparitive nanoindentation and macroindentation values found in literature; these were either magnitudes higher (Ebenstein) or about 50% lower (Czerner). It is intersting to note that ultimately the shape of the puncture curve as well as the max puncture force is the most relevant information for recommending the most appropriate surrogate material. Regardless of how similar the elasticity, reduced modulus or elastographic modulus of the surrogates are to the actual fibrotic tissue in the occluded arteries, they did not suitably mimic the behavior of the fibrotic tissue under the localized force of the guide wire.

Following the database creation and after analyzing all the quantitative and qual-

itative data obtained on the various potential surrogates, only two displayed the most similar properties as applied to clinically-relevant testing of the crossing device. These two surrogates are the bovine pericardium and the chicken skin, with preference to the bovine pericardium, however for cost-constraints and availability reasons, the chicken skin would best be suitable.

Table 7: Surrogate database and their compiled measured mechanical properties

Surrogate	**Nanoindentation** E_r (kPa)	**Elastography** $E(kPa)$	$E_r(kPa)$ **(Literature)**	**Max Puncture** (N)
Dense fibrotic tissue in CTO	52 ± 17.1	38.9	Thawed fibrotic tissue: 280 $(Range: 80-660)$ [33]	3.2
Medium fibrotic tissue in CTO	23 ± 5	27	–	3
Med-Loose fibrotic tissue in CTO	14 ± 1	27	Thawed hematoma: 240 $(Range: 60-1140)$ [33]	2.1
SynDaver soft occlusions	38	33 ± 3.35	–	1.1
Perma-Gel	69 ± 10.5	$-^*$	–	0.25
5% Agarose	406 ± 29.2	36*	840 ± 40[22]	0.2
20% Type A Porcine Gelatine	101 ± 11.6	$-^*$	$E = 67$ (macro-indentation spherical tip) [34]	0.71
Ginger	387 ± 31.9	–	–	n/a
Chicken skin	–	–	–	2.4
Fixed bovine pericardium	–	–	–	2.9
Pepperoni	–	–	–	1.25
Mozzarella	–	–	–	0.16
Tofu	–	–	–	0.76
Jujubes	–	–	–	0.61

**Elastography results for Perma-Gel, 5% Agarose and 20% Gelatine were not possible due to the gels being too transparent. Would need to incorporate scatterers.*

4.5 Limitations and Possible Sources of Error

Given the nature of studying biological tissue in ex-vivo conditions, there are consequently several non-ideal limitations. Evidently, the primary limitation in this research was the small pool of occluded arteries, in addition to lack of patient-to-patient sample variability; two of the three arteries that were viable fibrotic candidates were from the same donor. Second to this limitation was the lack of access to fresh tissue. The arteries were shipped to the SoundBite lab snap frozen after being harvested from a cadaver, most likely several hours post-mortem and not as fresh as desired. The arteries were also subjected to multiple thaw-freeze cycles during the study, with some damage becoming evident towards the final tests, where some arteries appeared to be slightly more crystalline. It is also uncertain as how exactly the mechanical properties could have changed during these multiple thaw-freeze cycles or during handling. The most evident effect of manipulating the samples was the fragility of the calcified walls which were intact when imaged at the micro-CT phase, however, some of the walls of the samples were observed to have been crushed immediately following the segmentation of the arteries into the 1.3 - 1.5 cm samples. A possible outcome of these premature wall fragmentations could possibly have explained lower-than-expected puncture peak loads or even a lowered reduced moduli. Another important limitation involved the puncture force test, where the short-lengthened samples were held in the absence of any tortuosity, axially aligned and radially reinforced so as to mimic the mechanical support of the arteries in vivo, however, there was no knowledge nor quantification of how much axial and radial support was needed to provide realistic compression during the tests, it was simply known that a standalone artery was impossible to puncture and extract any useful measurements.

5 Conclusions and Future Work

5.1 Conclusions

The development of fibrous tissue surrogates capable of mimicking the mechanical behavior of said tissue in CTOs are key to accelerating the development of new PCI technologies and interventional strategies. In this thesis, samples of occlusions containing fibrous-rich plaques were investigated and subjected to mechanical testing. A deeper understanding of fibrous tissue under compression of a wire was obtained and paved the way towards outlining specifications of an ideal surrogate. Potential surrogates, some artificial, others biological tissue, were examined, indented and punctured to create a synthetic and biological database of surrogate model viability, outlining mechanical properties and load-displacement behaviors. Importantly, it was demonstrated that the most relevant test for guiding the design of a CTO surrogate is the puncture force test, where the clinical application is most closely mirrored in the lab. The mechanical characterization values obtained such as elasticity, reduced modulus, hardness, etc., were not necessarily linked to finding the best surrogate.

It was shown that artificial surrogates (those investigated) offer many practical advantages over biological tissue, in terms of reproducibility, availability, visibility, however, there are important differences between wire-tissue and wire-substance interaction. Silicone, gel or elastomeric phantoms exhibit excessive frictional force between the initial puncture and the final boundary puncture and rupture differently than does a biomaterial with a rich web of collagen type I and III, elastin and hyaluronan. Drawbacks aside, most of these materials have the ability to be molded into the shape of a tortuous occlusion, so they are still somewhat still useful, either as experimental controls or as a filler matrix material for future complete CTO models. Out of the surrogates investigated, the two with the highest viability were animal tissues: bovine pericardium and chicken skin. They ruptured similarly to the fibrous tissue; under the controlled compressive force of

a straight 0.013" tuning wire, both the tissues followed a hyperelastic response to load and when the barrier was punctured, both produced near-zero instantaneous loads and displayed similar recoil behavior to the fibrous tissue in CTOs. Disadvantages do exist with these two surrogates; both of these materials have an inherent variability built-in, some samples may be thicker than others while some may have different ratios of collagen, elastin or hyaluronan. Additionally, these surrogates exist as sheet-like specimens, which structurally do not resemble fibrous-rich CTOs, in which fibrous tissue can be found densely anchored to the calcified or stiffened muscular walls in a layered fashion or matrixed with a thrombus or as a thickened proximal occlusion boundary.

Bovine pericardium and chicken skin demonstrated the most similar mechanical characteristics and compressive behavior to the fibrous tissue and for these reasons, it is this thesis' recommendation that chicken skin and bovine pericardium (if available) be used in the SoundBite lab as initial surrogates to experiment with Active Wire^{TM} and other new crossing technologies they have in development.

5.2 Future Work

Due to the complexity and heterogeneity of fibrotic tissue found in CTOs, this research could be complimented with a several additional studies to support the recommended material or propose a better surrogate, be it artificial or biological tissue. Firstly, additional investigative work should be carried out examining the viability of other surrogates, especially artificial surrogates, as it is more desirable in a controlled experiment setting. Suitable surrogates to explore include various hydrogels: collagen, cellulose, chitosan or alginate hydrogels, most of which would have to be modified or cross-linked to increase the strength and elastic recoil under compression. Additional surrogates could potentially come from electrospinning connective tissue subunits to create a visco-elastic material with tunable properties. Secondly, more work needs to be done to characterize the adhesive strength

and anchoring properties of the fibrotic tissue within CTOs. This will help distinguish the force required to puncture the material as opposed to tearing the material from it's surroundings. This is a critical piece of information for developing a more robust, realistic surrogate. Thirdly, more puncture testing and characterization validations could be performed on occluded specimens from other donors as this would provide a more diverse pool of fibrotic tissue and help with minimizing the sample bias. Lastly, for SoundBite purposes, the next step, once a fibrotic surrogate has been accepted, would be a study quantifying the energy required to cross fibrotic tissue or various thicknesses, density, compositions and to study the performance of the Active Wire^{TM} through the surrogate versus actual occlusions to confirm the surrogate performance.

References

[1] Ever D Grech. *ABC of interventional cardiology*, volume 196. John Wiley & Sons, 2011.

[2] Alfredo R Galassi, Emmanouil S Brilakis, Marouane Boukhris, Salvatore D Tomasello, Georgios Sianos, Dimitri Karmpaliotis, Carlo Di Mario, Bradley H Strauss, Stephane Rinfret, Masahisa Yamane, et al. Appropriateness of percutaneous revascularization of coronary chronic total occlusions: an overview. *European heart journal*, 37(35):2692–2700, 2015.

[3] Alfredo Bardají, Judit Rodriguez-López, and Mauricio Torres-Sánchez. Chronic total occlusion: to treat or not to treat. *World journal of cardiology*, 6(7):621, 2014.

[4] Julia Tucker De Sanctis. Percutaneous interventions for lower extremity peripheral vascular disease. *Am Fam Physician*, 64(12):1965–1973, 2001.

[5] Doo Sun Sim, Myung Ho Jeong, Kyoung Rae Cha, Suk Ho Park, Jong Oh Park, Young Min Shin, Heungsoo Shin, Young Joon Hong, Youngkeun Ahn, Robert S Schwartz, et al. A reliable porcine coronary model of chronic total occlusion using copper wire stents and bioabsorbable levo-polylactic acid polymer. *Journal of cardiology*, 60(6):443–447, 2012.

[6] Michael Frie, Michael Jorgenson, Mark E Smith, and Michael Conforti. A reproducible model of a chronic partial occlusion: A cylindrical bone marrow allograft implanted in the porcine coronary and peripheral vasculature. *Journal of Medical Devices*, 9(2):020909, 2015.

[7] Brian S Kates. Magnetic resonance elastography for measuring the compliance of chronic total occlusions. Master's thesis, University of Toronto, 2011.

[8] John A Ambrose and Manmeet Singh. Pathophysiology of coronary artery disease leading to acute coronary syndromes. *F1000prime reports*, 7, 2015.

[9] Timi grade flow - grading of coronary blood flow during coronary angiography | classifications, online calculators, and tables in radiology. http://radclass.mudr.org/content/timi-grade-flow-grading-coronary-blood-flow-during-coronary-angiography. (Accessed on 02/27/2018).

[10] Jacob Fog Bentzon, Fumiyuki Otsuka, Renu Virmani, and Erling Falk. Mechanisms of plaque formation and rupture. *Circulation research*, 114(12):1852–1866, 2014.

[11] Johannes A Schaar, James E Muller, Erling Falk, Renu Virmani, Valentin Fuster, Patrick W Serruys, Antonio Colombo, Christodoulos Stefanadis, S Ward Casscells, Pedro R Moreno, et al. Terminology for high-risk and vulnerable coronary artery plaques. *European heart journal*, 25(12):1077–1082, 2004.

[12] Yo-Han Park, Yong-Kyun Kim, Duck-Jun Seo, Young-Hoon Seo, Chung-Seop Lee, In-Geol Song, Dong-Ju Yang, Ki-Hong Kim, Hyun-Woong Park, Wan-Ho Kim, et al. Analysis of plaque composition in coronary chronic total occlusion lesion using virtual histology-intravascular ultrasound. *Korean circulation journal*, 46(1):33–40, 2016.

[13] Yoshiki Matsuo, Takuro Takumi, Verghese Mathew, Woo-Young Chung, Gregory W Barsness, Charanjit S Rihal, Rajiv Gulati, Eric T McCue, David R Holmes, Eric Eeckhout, et al. Plaque characteristics and arterial remodeling in coronary and peripheral arterial systems. *Atherosclerosis*, 223(2):365–371, 2012.

[14] Louis-Philippe Riel, Steven Dion, Martin Brouillette, Simon Bérubé, Marc-Antoine Despatis, and Etienne Bousser. Characterization of calcified plaques retrieved from occluded arteries and comparison with potential artificial analogues. *International Mechanical Engineering Congress and Exposition*, (IMECE2014-38152), 2014.

[15] Ronen Jaffe, General Leung, Nigel R Munce, Amandeep S Thind, Howard Leong-Poi, Kevan JT Anderson, Xiuling Qi, Judy Trogadis, Ariella Nadler, Davida Shiff, et al. Natural history of experimental arterial chronic total occlusions. *Journal of the American College of Cardiology*, 53(13):1148–1158, 2009.

[16] How does a micro-ct scanner work? | micro photonics. https://www.microphotonics.com/how-does-a-microct-scanner-work/. (Accessed on 03/08/2018).

[17] Tobias De Zordo, Stephanie R Lill, Christian Fink, Gudrun M Feuchtner, Werner Jaschke, Rosa Bellmann-Weiler, and Andrea S Klauser. Real-time sonoelastography of lateral epicondylitis: comparison of findings be-

tween patients and healthy volunteers. *American Journal of Roentgenology*, 193(1):180–185, 2009.

[18] Nathalie Ganne-Carrié, Marianne Ziol, Victor de Ledinghen, Catherine Douvin, Patrick Marcellin, Laurent Castera, Daniel Dhumeaux, Jean-Claude Trinchet, and Michel Beaugrand. Accuracy of liver stiffness measurement for the diagnosis of cirrhosis in patients with chronic liver diseases. *Hepatology*, 44(6):1511–1517, 2006.

[19] Cobbold RS. *Foundations of biomedical ultrasound*. Oxford University Press, New York, 2007.

[20] E. Dieulesaint and D. Royer. *Elastic waves in solids I: free and guided propagation*. Springer Verlag, New York, 2000.

[21] Anthony C Fischer-Cripps. *Contact mechanics*. Springer, 2011.

[22] DM Ebenstein and LA Pruitt. Nanoindentation of soft hydrated materials for application to vascular tissues. *Journal of Biomedical Materials Research Part A*, 69(2):222–232, 2004.

[23] Constance L Slaboch, Mark S Alber, Elliot D Rosen, and Timothy C Ovaert. Mechano-rheological properties of the murine thrombus determined via nanoindentation and finite element modeling. *Journal of the mechanical behavior of biomedical materials*, 10:75–86, 2012.

[24] Nick Wang. Biomechanics of diseased aorta tissue: Indentation. Master's thesis, McGill University, 2017.

[25] Duanjie Li and Jorge Ramirez. *Hydrogel Mechanical Properties Using Nanoindentation*. Nanovea, 6 Morgan, Ste 156, Irvine CA 92618, 2017. (Accessed on 02/27/2018).

[26] W. C. Oliver and G. Pharr. An improved technique for determining hardness and elastic modulus using load and displacement sensing indentation experiments. *Journal of Materials Research*, 7(6):1564–1583, 1992.

[27] Astm f2394 - 07(2017) standard guide for measuring securement of balloon expandable vascular stent mounted on delivery system. https://www.astm.org/Standards/F2394.htm, 2017. (Accessed on 02/28/2018).

[28] Astm f1306 - 16 standard test method for slow rate penetration resistance of flexible barrier films and laminates. https://www.astm.org/Standards/F1306.htm. (Accessed on 02/27/2018).

[29] Darryl Amick. Gel compositions as muscle tissue simulant and related articles and methods, May 24 2007. US Patent App. 11/452,660.

[30] Tiffany Christina Zigras. *Biomechanics of Human Pericardium: A Comparative Study of Fresh and Fixed Tissue*. PhD thesis, McGill University, 2007.

[31] S Cliche, J Amiot, C Avezard, and C Gariepy. Extraction and characterization of collagen with or without telopeptides from chicken skin. *Poultry science*, 82(3):503–509, 2003.

[32] Peter Takizawa. Connective tissue.

[33] Donna M Ebenstein, Dezba Coughlin, Joan Chapman, Cheng Li, and Lisa A Pruitt. Nanomechanical properties of calcification, fibrous tissue, and hematoma from atherosclerotic plaques. *Journal of biomedical materials research Part A*, 91(4):1028–1037, 2009.

[34] Marina Czerner, Lucas Sanchez Fellay, María P Suárez, Patricia M Frontini, and Laura A Fasce. Determination of elastic modulus of gelatin gels by indentation experiments. *Procedia Materials Science*, 8:287–296, 2015.

[35] Bradley H Strauss, Lorne Goldman, Beiping Qiang, Nafiseh Nili, Amit Segev, Jagdish Butany, John D Sparkes, Zane S Jackson, Mohammad R Eskandarian, and Renu Virmani. Collagenase plaque digestion for facilitating guide wire crossing in chronic total occlusions. *Circulation*, 108(10):1259–1262, 2003.

[36] CB Raub, AJ Putnam, BJ Tromberg, and SC George. Predicting bulk mechanical properties of cellularized collagen gels using multiphoton microscopy. *Acta biomaterialia*, 6(12):4657–4665, 2010.

[37] Kenichi Sakakura, Masataka Nakano, Fumiyuki Otsuka, Kazuyuki Yahagi, Robert Kutys, Elena Ladich, Aloke V Finn, Frank D Kolodgie, and Renu Virmani. Comparison of pathology of chronic total occlusion with and without coronary artery bypass graft. *European heart journal*, 35(25):1683–1693, 2013.

[38] S Johnson, S Duffy, G Gunning, M Gilvarry, JP McGarry, and PE McHugh. Review of mechanical testing and modelling of thrombus material for vascular implant and device design. *Annals of biomedical engineering*, 45(11):2494–2508, 2017.

[39] Aimée Sakes, Evelyn Regar, Jenny Dankelman, and Paul Breedveld. Crossing total occlusions: navigating towards recanalization. *Cardiovascular engineering and technology*, 7(2):103–117, 2016.

[40] Kelly Mônica Marinho e Lima, José Francisco Silva Costa Júnior, Wagner Coelho de Albuquerque Pereira, and Liliam Fernandes de Oliveira. Assessment of the mechanical properties of the muscle-tendon unit by supersonic shear wave imaging elastography: a review. *Ultrasonography*, 37(1):3, 2018.

[41] KC McGilvray, R Sarkar, and CM Puttlitz. Mechanical characterization of deep vein thrombosis in a murine model using nanoindentation. *WIT Transactions on Biomedicine and Health*, 13:57–67, 2009.

[42] Mark Ahearne, Eleftherios Siamantouras, Ying Yang, and Kuo-Kang Liu. Mechanical characterization of biomimetic membranes by micro-shaft poking. *Journal of The Royal Society Interface*, 6(34):471–478, 2009.

[43] S Sanjay Srivatsa, William D Edwards, Christine M Boos, Diane E Grill, Giuseppe M Sangiorgi, Kirk N Garratt, Robert S Schwartz, and David R Holmes. Histologic correlates of angiographic chronic total coronary artery occlusions: influence of occlusion duration on neovascular channel patterns and intimal plaque composition. *Journal of the American College of Cardiology*, 29(5):955–963, 1997.

[44] Acute coronary syndromes. https://foamdation.com/2017/05/16/acute-coronary-syndromes/. (Accessed on 02/27/2018).

[45] Rebecca G. Wells. Tissue mechanics and fibrosis. *Biochimica et Biophysica Acta*, 1832(7):884–890, 2013.

6 Appendix

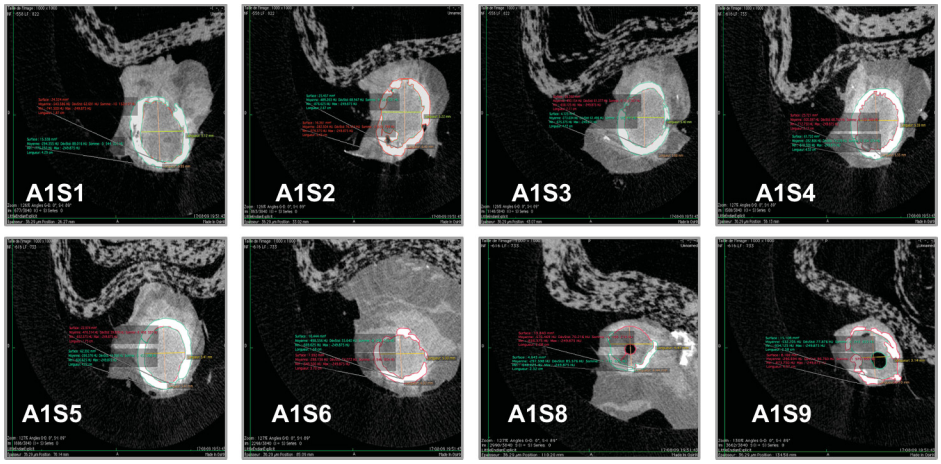

Figure 26: Micro-CT snapshots of each proximal segment of A1

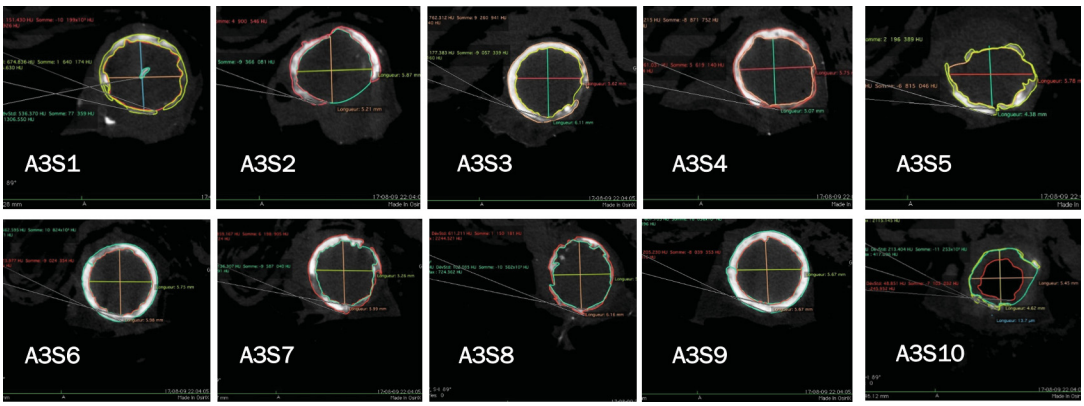

Figure 27: Micro-CT snapshots of each proximal segment of A3

Table 8: Detailed micro-CT notes for A1 and A3

(a) A1 micro-CT observations. A1 length is 11.58cm

Location (mm)	**Notes (Dr. Soulez)**	**True Location (mm)**
19.739	Proximal start, permeable region however partially occluded	0
26.271 - 53.957	Completely occluded	6.532 to 34.218
49.204	Fresh thrombus, looks liquid	29.465
53.957	Completely thrombosed	34.218
53.957 - 97.972	Completely thrombosed	34.218 to 78.233
97.972	Permeable from this location distally with stenosis regions and plaques	78.233
110.418	Stenotic epicenter (most severe stenosis seen here)	90.679
117.058	Very permeable section of artery	97.319
124.859 - 130.774	Second severe stenosis with ulceration	105.12 to 111.035
130.774	Eccentric calcified plaque with stenosis	111.035
135.527	Distal end of artery	115.788

(b) A3 micro-CT observations. A3 length is 12.95 cm

Location (mm)	**Notes (Dr. Soulez)**	**True Location (mm)**
17.054	Proximal start of artery; it is occluded	0
23.018	Small calcification in thrombus	5.964
37.846	Thrombosed zone (liquid/soft)	20.792
44.259	Thrombosed zone (liquid/soft)	27.205
79.974	Calcified thrombus (large/central)	62.92
97.863	Calcified thrombus (small)	80.809
111.905	Calcified thrombus (small)	94.851
141.297	Permeable, not fully occluded until distal end of artery	124.243
146.558	Distal end of artery	129.504

Table 9: Corrected micro-CT density values (in HU) for artery 1 and 3 obtained for the luminal region and the wall

Segment	Z (mm)	Lumen (HU)	Wall (HU)
A1S1	26.3	47.4	296.6
A1S2	33.0	101.7	308.5
A1S3	43.1	100.8	317.4
A1S4	56.1	90.4	308.2
A1S5	70.1	114.7	324.4
A1S6	85.1	92.4	302.9
A1S7	97.1	49.8	301.4
A1S8	110.2	14.5	293.4
A1S9	134.6	58.3	294.3
A3S1	22.3	92.5	908.6
A3S2	34.5	102.6	1513.3
A3S3	53.3	159.0	1784.1
A3S4	68.8	142.1	1603.8
A3S5	82.7	105.2	1180.1
A3S6	93.0	160.0	1797.9
A3S7	107.0	132.2	1375.5
A3S8	120.1	75.1	893.0
A3S9	133.0	210.4	2054.7
A3S10	146.1	108.3	642.4

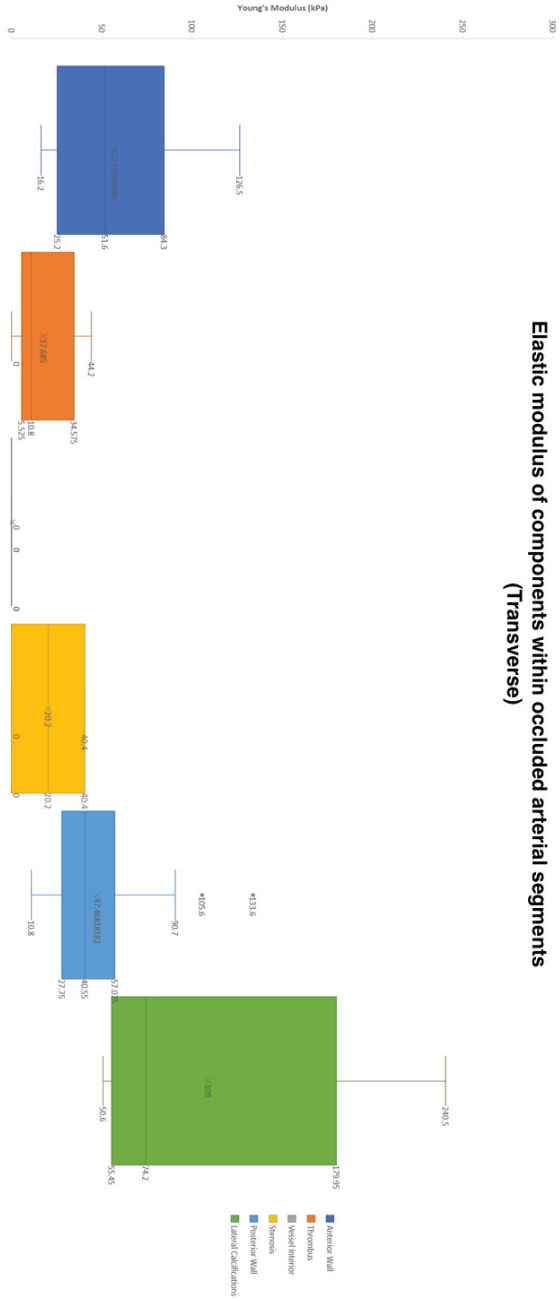

Figure 28: Transverse elastic modulus measurements of components within occluded arterial segments

Table 10: Correlation of E and SD with plaque composition and histological findings for arteries 2 and 3

Segment	**E (kPa)**	**SD**	**Predicted Composition**	**Elastic-Histological Findings**
A3S1	44.2	4.3	Homogenous	Fragmented calcium in wall, fragmented thrombus. Elastic value suggests homogenous, possibly fibrothrombotic
A3S2	11.6	6.9	Heterogenous	Less dense signal on micro-CT, suggests softer, closer to liquid composition. The middle of the lumen shows less organization with a high degree of heterogeneity
A3S3	5.9	3	Heterogenous	Histological findings suggest a medium to loosely packed fibrous lumen, but there is discordance with elastic values possibly due to the calcific walls obscuring the measurement
A3S4	0	0	n/a	Discordance with elastography measurements. Should be dense to loose fibrotic tissue values (closer to 40 kPa) – might have been mistaken for segment 5 – re-verify when puncturing
A3S5	33.6	3.4	Homogenous	Histology slide is not usable, it stained damaged tissue after the cut. Micro-CT shows completely calcified wall. Again, must re-verify and observe when puncturing
A3S6	8.8	8	Heterogenous	Extremely heterogenous elastic values. Histology shows a small intact section that is of medium density fibrotic tissue. Remainder of the lumen was damaged and no further conclusions can be made
A3S7	0	0	n/a	Match maybe with segment A3S8. Histological analysis shows intermediate, loose connective tissue. Slightly thrombotic. Elastic values are discordant – could be due to calcifications (however micro-CT doesn't show substantial luminal calcium in this localized area)
A3S8	8.1	4.2	Heterogenous	More consistent findings in histology with elastic values of segment A3S9. Highly variable, shows a mix of loose to medium density fibrous tissue, fragments of calcium and possibly some cholesterol clefts
A3S9	12.8	4	Heterogenous	Air; unreliable quantities measured in elasto
A3S10	2.6	3.2	Heterogenous	No A3S10 stained in histology, was used as a test segment
A2S2	20.7	20.8	Heterogenous	Histology slide was damaged due to high calcification
A2S3	0	0	Air	No elastic or histological conclusions can be drawn
A2S5	0	0	Air	No elastic or histological conclusions can be drawn

Table 11: Summary of puncture results for all surrogates examined

Surrogate Punctured	**Notes**	**Potentially Suitable?**
Perma-Gel	Repeatable, moldable, easy to prepare	only as an experimental control
Gelatine	Stiffness inconsistency with recipe, mold grows easily on it	no - a collagen hydrogel with tunable stiffness would be better, however would lack heterogeneity
Jujubes	Glucose residue builds up on wire, not easy to work with, too soft	No
Mozzarella	Too soft and porous	No
Extra firm smoked tofu	Too soft and porous	No
Various pepperoni and sausages	Very heterogenous, need stiffer sausages, sample variability is potential issue	Yes - for complete occlusion if can stiffen the contents of the sausage
Syndaver soft occlusion	Not stiff enough, not very heterogenous, puncture curve similar to Perma-Gel	No - not heterogenous enough as a hydrogel, not a similar puncture mechanism
Syndaver hard occlusion	Experimental setup broke, it was too hard to puncture	No - too hard for fibrotic tissue
Glutarhydrate-fixed bovine pericardium	Modified jig required, has to be punctured in layers	Yes - shows repeatable puncture curves, similar load increase to med to dense fibrotic tissue
Chicken skin	Modified jig required, has to be punctured in layers, cheap and easier to procure than bovine pericardium	Yes - shows repeatable puncture curves, similar load increase to med to dense fibrotic tissue